

Robust optimization of CO₂ Sequestration through a water alternating gas process under geological uncertainties in Cuu Long Basin, Vietnam

Thanh, Hung Vo

Department of Earth Resources Engineering, Graduate school of Engineering, Kyushu University

Sugai, Yuichi

Department of Earth Resources Engineering, Faculty of Engineering, Kyushu University

Nguele, Ronald

Department of Earth Resources Engineering, Faculty of Engineering, Kyushu University

Sasaki, Kyuro

Department of Earth Resources Engineering, Faculty of Engineering, Kyushu University

<https://hdl.handle.net/2324/4354920>

出版情報 : Journal of Natural Gas Science and Engineering. 76, pp.103208-, 2020-04-01. Elsevier

バージョン :

権利関係 :

1 Title of paper

2 **Robust optimization of CO₂ Sequestration through a water alternating gas process**
3 **under geological uncertainties in Cuu Long Basin, Vietnam**

4
5
6 Hung Vo Thanh*, Yuichi Sugai, Ronald Nguele and Kyuro Sasaki

7
8
9
10 Department of Earth Resources Engineering, Faculty of Engineering, Kyushu University,

11 744 Motooka Nishi-ku, Fukuoka 819-0395, Japan

12

13

14 * Corresponding author

15 Email: vothanhhung198090@gmail.com

16 Tel: +8150-6872-1708

17

18

19

20

21

22

Abstract

This study presents a robust optimization workflow to determine the optimal water alternating gas (WAG) process for CO₂ sequestration in a heterogeneous fluvial sandstone reservoir. As depicted in this study, WAG injection could enhance CO₂ residual and solubility trapping based on an integrated modeling workflow. First, continuous CO₂ injection and WAG were compared to demonstrate the efficiency of the WAG process for CO₂ trapping enhancement. To achieve this while highlighting the impact of reservoir heterogeneity, 200 geological realizations were generated considering a wide range of plausible geological conditions. The ranking of these realizations was performed by quantifying the CO₂ cumulative injection (P10, P50, and P90 realizations) that represent the overall geological uncertainties. Then, an innovative robust workflow was used Artificial Intelligence optimizer to determine the optimal solution for CO₂ trapping. For comparison, a nominal optimization workflow of P50 realization was also conducted. The proposed robust optimization workflow resulted in higher CO₂ trapping than the nominal optimization workflow. Thus, this study demonstrates a fast and reliable workflow that can accurately represent for optimization the cycle length injection in the WAG process under geological uncertainties.

17

18 **Keywords:** Artificial Intelligence, CO₂ sequestration, geological uncertainties, robust
19 optimization, trapping mechanism, WAG process

20

21

22

23

24

25

1 **1. Introduction**

2 Geological CO₂ storage (GCS), whereby CO₂ is collected from industrial sources and
3 injected into deep geological formations, is one of the most remarkable potential technologies
4 for reducing greenhouse-gas emissions in the atmosphere (IPCC, 2005). Possible storage
5 formations include depleted oil and gas reservoirs, coal beds, and deep saline aquifers (Bachu,
6 2000). Among these formations, saline aquifers have the largest CO₂ storage capacity (Lackner,
7 2003). However, economic and environmental concerns related to CO₂ sequestration in saline
8 aquifers must be addressed before large-scale CO₂ sequestration can occur (Bruant et al., 2002;
9 IPCC, 2005). Typically, CO₂ is injected into saline formations as a dense, low-viscosity
10 supercritical fluid (scCO₂) at a minimum depth of 800 m to optimize storage efficiency (Bachu,
11 2002; Holloway and Savage, 1993; Iglauer et al., 2011). After injection, scCO₂ rises upward
12 as a result of buoyancy until it reaches an impermeable zone (Flett et al., 2007; Hassanzadeh
13 et al., 2009).

14 Four recognized trapping mechanisms have been reported to halt the upward movement of
15 the CO₂ plume within a saline aquifer. The first trapping mechanism is structural or
16 stratigraphic trapping through entrapment under an impermeable layer of cap rock (Hesse and
17 Woods, 2010; Naylor et al., 2011). The second trapping mechanism is residual trapping,
18 whereby CO₂ is trapped in the pore space between rock grains (Juanes et al., 2006; Kumar et
19 al., 2005). This trapping mechanism is considered the most rapid method to remove CO₂ from
20 its free phase within stipulated time scales (from years to decades) (Ennis-King and Paterson,
21 2005; Kumar et al., 2005; Shamshiri and Jafarpour, 2012). During the displacement, the front
22 and tail of the CO₂ plume move per the drainage and imbibition process (Doughty, 2007). CO₂
23 residual trapping in porous media is dependent on the initial gas saturation at the beginning of
24 imbibition and the saturation history of the porous media (Doughty, 2007; Juanes et al., 2006);

1 thus, residual trapping is more effective with increasing contact between CO₂ and the fresh part
2 of the storage formation (B.J.O.L. McPherson and Cole, 2000).

3 The third trapping mechanism is the dissolution of CO₂ in the formation brine (Meng and
4 Jiang, 2014; Span and Wagner, 1996; Spycher and Pruess, 2005; Yan et al., 2011). This
5 mechanism (also known as solubility trapping) can improve CO₂ storage security as the rate of
6 CO₂ leakage is minimal. The importance of CO₂ solubility trapping led to the theoretical (Span
7 and Wagner, 1996), experimental (Spycher and Pruess, 2005; Yan et al., 2011), and numerical
8 analyses (Meng and Jiang, 2014) of this mechanism. For instance, Span and Wagner (1996)
9 proposed a new equation of state for carbon dioxide at the focus region at high temperatures
10 and pressures (up to 1100 K and 800 MPa, respectively). Furthermore, Spycher and Pruess
11 (2005) determined the mutual solubility of CO₂–H₂O (from 12–100 °C and up to 600 bar) to
12 investigate the effect of chloride salts in the aqueous phase. Moreover, Yan et al. (2011)
13 measured the densities of CO₂ in 0, 1, and 5 mol/kg NaCl brines at 323, 373, and 413 K and a
14 pressure range from 5 MPa to 40 MPa. Their results indicated that dissolved CO₂ increases
15 brine density only if the apparent mass density of CO₂ in the brine is higher than the brine
16 density under the same conditions.

17 The fourth trapping mechanism is mineral trapping, whereby the injected CO₂ can be
18 permanently stored in the aquifer as a result of chemical reactions between the CO₂ and brine
19 aquifer to create solid-phase minerals (Bachu et al., 1994; Xu et al., 2004). In the present
20 research, the mineral trapping mechanism was not considered because it is considerably slower
21 than the residual and solubility trapping mechanisms (Gaus, 2010). The efficiency of these
22 CO₂-trapping mechanisms depends on a variety of factors, including reservoir heterogeneities
23 (Dai et al., 2018), cap rock properties (Iglauer et al., 2015), CO₂–rock wettability (Al-
24 khdheeawi et al., 2018; Al-Menhal et al., 2015; Iglauer, 2017), brine salinity (Al-Khdheeawi

1 et al., 2018b, 2017), reservoir temperature, and wettability heterogeneity (Al-khdheewi et al.,
2 2018).

3 Recently, CO₂-enhanced oil recovery (EOR) has been considered an important economic
4 incentive in the early stage of carbon capture and storage (CCS) projects (Dai et al., 2016; Mac
5 Dowell et al., 2017). Dai et al. (2016) proposed an integrated statistical framework by applying
6 geostatistic-based Monte Carlo simulations to evaluate the CO₂-storage potential and economic
7 analysis at the Farnsworth Unit, Texas. Moreover, Mac Dowell et al. (2017) stated that CO₂-
8 EOR is a promising technology for cost reduction and climate change mitigation.

9 In addition, numerical simulation studies are useful tools for evaluating the performance
10 of CO₂-EOR and storage. However, geological uncertainties (e.g., permeability, porosity) have
11 strong impact on reservoir simulation results. **Geological uncertainties are an inherent**
12 **characteristic of the petroleum exploration process. The uncertainty can be related to**
13 **subsurface data and interpretation of those data (CMG, 2019)**. Finding an optimal
14 simulation result using optimization algorithms is a potential way of reducing these
15 uncertainties (Sibawihi et al., 2015).

16 Optimization under geological uncertainties have been proposed in several studies (Dang
17 et al., 2016; Foroud et al., 2016; Nguyen et al., 2016; Nwachukwu et al., 2018; Welkenhuysen
18 et al., 2017). However, these studies emphasize on optimizing oil production performance
19 rather than CO₂ sequestration.

20 Several studies have focused on the co-optimization of sequestration and CO₂-EOR
21 (Eshraghi et al., 2016; Ettehad tavakkol et al., 2014; Li et al., 2016; Min et al., 2018; Safarzadeh
22 and Motahhari, 2014). These authors used limited data and simple models to introduce their
23 workflow. Li et al. (2016) used numerical compositional modeling on a sector model in
24 Shanbei, China by utilizing the response surface method to maximize the profit and amount of
25 CO₂. However, a few numerical simulation studies of CO₂ sequestration and EOR emphasized

1 on incorporating geological uncertainties into an optimization framework. Ampomah et al.
2 (2017) proposed the framework for the co-optimization of CO₂-EOR and storage through the
3 WAG process under geological uncertainty. These authors concluded that the optimization
4 framework improves the amount of CO₂ storage up to 94% that can increase oil recovery by
5 approximately 25%.

6 Water alternating gas (WAG) is an effective method that enhances CO₂ trapping and
7 sequestration (Al-Khdheeawi et al., 2018a). This study showed that WAG technology reduced
8 CO₂ mobility and improved trapping capacity.

9 Furthermore, WAG improves residual and solubility trapping compared with continuous
10 CO₂ injection (Rasmusson et al., 2016; Spiteri et al., 2005). However, consistent and effective
11 optimization of the WAG injection process requires a strategy for finding the most effective
12 injection rates and cycle length for CO₂ trapping. Zhang and Agarwal (2013) proposed an
13 optimization method based on a genetic algorithm to determine the water and CO₂ injection
14 rates resulting in the optimal level of solubility trapping. Nevertheless, the authors did not
15 consider the effects of gas and cycle length under geological uncertainties on this optimization
16 process. Geological uncertainties exhibit notable effects on the behavior of injected CO₂
17 (Aminu et al., 2017; Welkenhuysen et al., 2017). Therefore, the impact of geological
18 uncertainties must be adequately considered before a robustly optimal CO₂ sequestration
19 solution can be ascertained.

20 Previous studies have integrated modeling and robust optimization approach to determine
21 optimal solutions while considering uncertainties in geological constraints. This approach,
22 including low-salinity WAG process (Dang et al., 2016), alkaline-surfactant-polymer flooding
23 (Dang et al., 2018), gas-assisted gravity drainage (GAGD) process (Al-Mudhafar et al., 2018),
24 unconventional reservoirs (Nguyen et al., 2016), well placement optimization (Jesmani et al.,
25 2020), water flooding optimization (Pinto et al., 2019; Yasari and Pishvaie, 2015), steam-

1 assisted gravity drainage process (Fedutenko et al., 2013; Yang et al., 2011), has been applied
2 in various improved oil recovery/EOR studies. However, the effect of robust optimization on
3 CO₂ sequestration using WAG injection has not been addressed.

4 Therefore, the present study proposes an optimization framework to maximize field-scale
5 trapping of CO₂ using the WAG process while also considering the effects of geological
6 uncertainties on the model results. The studied field reservoir is a heterogeneous sandstone
7 reservoir in the Nam Vang oilfield located offshore of Vietnam (Vo Thanh et al., 2019b). The
8 reservoir is thought to be fully depleted and 100% brine-saturated from the surrounding
9 aquifers.

10 To the best of our knowledge, we present one of the first studies on the integrated modeling
11 and robust optimization of field-scale CO₂ sequestration processes with the following
12 objectives:

- 13 • Determining the optimal solution to maximize residual and solubility trapping of CO₂
14 by varying the injection cycle length during the WAG process;
- 15 • Presenting a robust optimization based on artificial intelligence (AI) workflow to
16 account for the overall geological uncertainties of reservoir characteristics during
17 CO₂ injection and trapping;
- 18 • Establishing a comparison between the designed robust optimization workflow and
19 traditional nominal optimization techniques in terms of optimal water and gas cycle
20 length in the WAG process conditioning to the geological realizations.

21 **2. CO₂-WAG sequestration process**

22 WAG injection is a popular EOR technique. This method entails injecting a slug of gas (CO₂)
23 into the reservoir alternating with water. Water injection is used to control the mobility of the
24 gas to improve the sweep efficiency, and gas injection enhances the microscopic displacement

efficiency (Christensen et al., 2001). Optimization of the WAG process-EOR minimizes the total amount of injected gas required to dissolve hydrocarbons (Song et al., 2014). WAG technology has been proposed to enhance oil recovery and carbon storage because of its capability to improve macroscopic and microscopic sweep efficiencies in hydrocarbon reservoirs (Zhong et al., 2019). Furthermore, carbonation and mineralization occur during WAG injection into reservoir formations, and thus CO₂ can be sequestered. Despite numerous chemical reactions are associated with WAG injection into reservoir formations, the present study only considered the physical aspect of the WAG process. An effective improvement of solubility and residual trapping was observed during WAG optimization for CO₂ sequestration. This improvement could potentially offset the costs of water injection. This improvement was achieved by optimizing the alternating cycles of injection. One WAG cycle is defined as a complete cycle of CO₂-water injection (Zhang and Agarwal, 2013). **Figure 1** illustrates the recognized WAG operations. The yellow and green blocks represent CO₂ and water injections, respectively, and the width of blocks indicates the injection period.

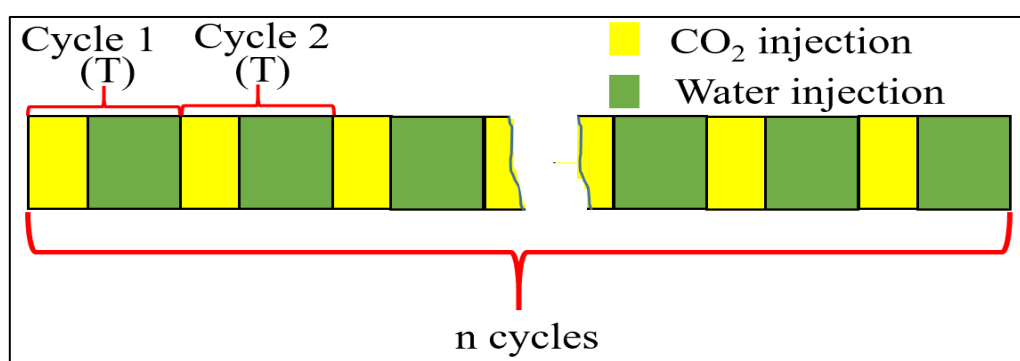


Figure 1. Schematic of the WAG process for CO₂ sequestration

1 **3. Geological background**

2 Cuu Long Basin is a tertiary extensional basin formed as the result of Indochina's extrusion
3 along Three Pagodas Fault and Red River Fault because of the collision of India to Eurasia
4 during Paleocene (Morley, 2002). This basin is the largest basin in offshore Vietnam. The basin
5 is formed on the pre-Cenozoic active regression continent crust and filling with Late Cenozoic
6 passive continent margin sediments (Hung and Le, 2004).

7 The tectonic event of Cuu Long Basin can be classified into the following five main stages
8 (Schmidt et al., 2019):

- 9 • Stage 1: The pre-rift uplift was found on Late Cretaceous–Eocene.
- 10 • Stage 2: The main rift phase was filled with Late Eocene–Oligocene to develop the main
11 structural features within the basin to follow the extensional and transtensional
12 deformations.
- 13 • Stage 3: Regional subsidence was found on Early Middle Miocene to mark by changing
14 from the fault-controlled subsidence to the high-rate subsidence.
- 15 • Stage 4: The partial inversion was filled with the Late Miocene. In this stage, the entire area
16 was dominated by compression and combination with the dextral strike-slip fault system in
17 east offshore Vietnam.
- 18 • Stage 5: The regional subsidence was found on Pliocene–Pleistocene to diversify the
19 tectonic activity ranging from low to moderate amplitudes with different uplifts across the
20 basin.

21 Nam Vang field, the study area, is geographically located in the northwestern margin in the
22 Cuu Long Basin, offshore southern Vietnam, approximately 160 km east of Vung Tau City
23 (**Figure 2a**) (Vo Thanh et al., 2019a). Oligocene sandstones and granite fractured reservoir are
24 the main reservoirs in Nam Vang field.

1 The reservoir target in this study is the Oligocene sandstone of Tra Tan formation. The Late
 2 Oligocene sediment source is more distal resulting in predominant mudstones with
 3 interbedding of sandstones. Depositional environments include fluvial in southwestern basin
 4 to lacustrine in northeastern basin. Hydrocarbons have been explored and exploited in the
 5 sandstone of E, C, BI.1, and BI.2 sequences. The good-source rock is indicated in the lacustrine
 6 shale of D and E sequences containing the large amount of total organic carbon and
 7 hydrocarbon index values. The general stratigraphic sequences of Nam Vang field are shown
 8 in **Figure 2b** (Vo Thanh et al., 2019a).

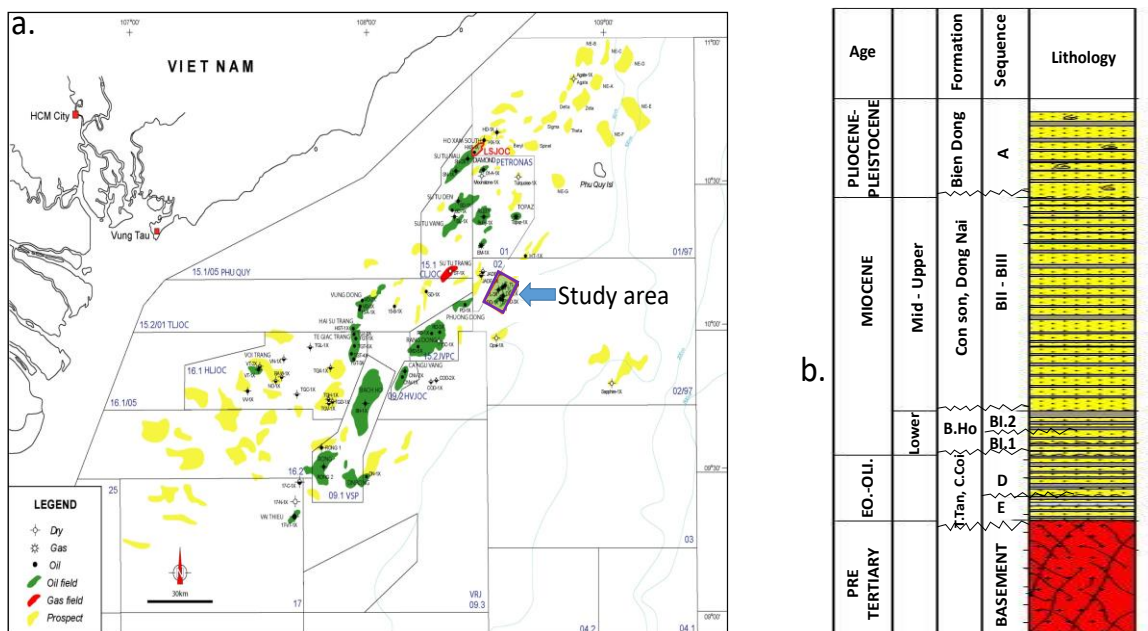


Figure 2. Study area (a) and general stratigraphy (b) for this study

9 4. Model description

10 Our proposed method for optimizing CO₂ sequestration using the WAG process was tested
 11 on a model of a heterogeneous sandstone reservoir in the Nam Vang oilfield offshore of
 12 Vietnam. No significant fractures or faults are present in this reservoir. Two lithology types
 13 (i.e., fluvial sand and shale deposits) were considered. Petrophysical properties and three-
 14 dimensional lithofacies were modeled using object-based modeling and sequential Gaussian
 15 simulation (Vo Thanh et al., 2019b).

1 The initial geological model comprised 2 604 800 grid cells with 148, 176, and 100 grids
2 in the I, J, and K directions, respectively. For field-scale reservoir simulations, consideration
3 was given to efficient computational time and CPU resources during the property upscaling
4 and gridding. Accordingly, root-mean-square upscaling was used to create a coarse grid
5 system for CO₂ flow simulation that allowed for smooth and quick simulations with the
6 available CPU resources. This system had 48 000 grid cells corresponding to 40, 48, and 25
7 grid cells in the I, J, and K directions, respectively.

8 Then, harmonic and arithmetic algorithms were used during the upscaling process to
9 preserve reservoir heterogeneity and corresponding variations in reservoir characteristics. The
10 model dimensions were 5000 m × 2000 m × 100 m (I × J × K). This model had a datum depth
11 of 2090 m at a pressure at 20.16 MPa for equilibrium initialization. Afterward, CO₂ was
12 injected at a temperature of 50 °C and at a depth of 2160 m. Rock compressibility was $5.2 \times$
13 10^{-5} kPa⁻¹.

14 For the CO₂ injection modeling, the compositional model (CMG-GEM) was used to
15 simulate the flow of two components (i.e., CO₂ and H₂O). This study chose the Brooks and
16 Corey model for the relative permeability curves (Brooks and Corey, 1964) and the Van
17 Genuchten function for the capillary pressure curve (Genuchten, 1980). Moreover, the
18 treatment of residual CO₂ trapping in the present work was based on the hysteresis model of
19 Land (Land, 1968). **Figure 3** depicts Land's residual trapping model adopted in this study.
20 Throughout this study, CO₂ injection and subsequent movement and storage within the
21 reservoir were considered in the absence of geochemical considerations and mean mineral
22 trapping.

23

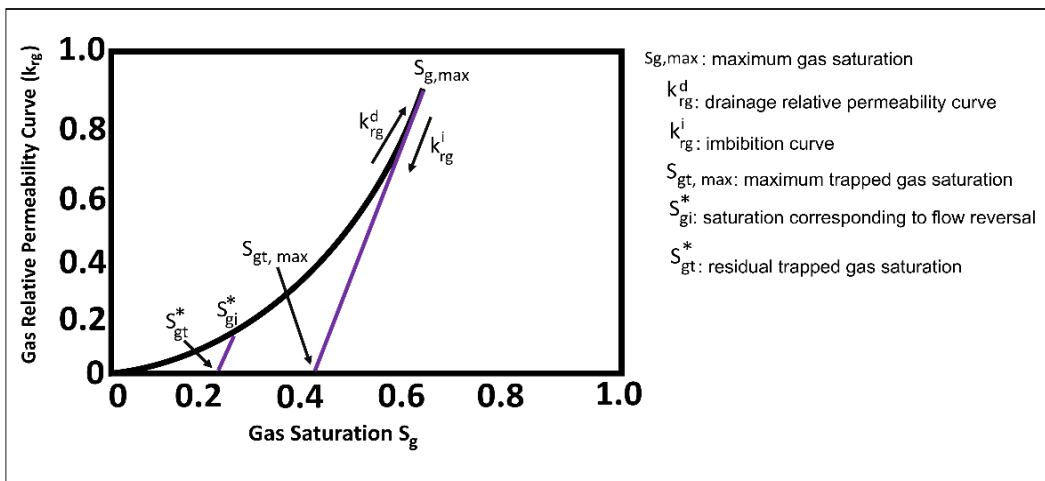
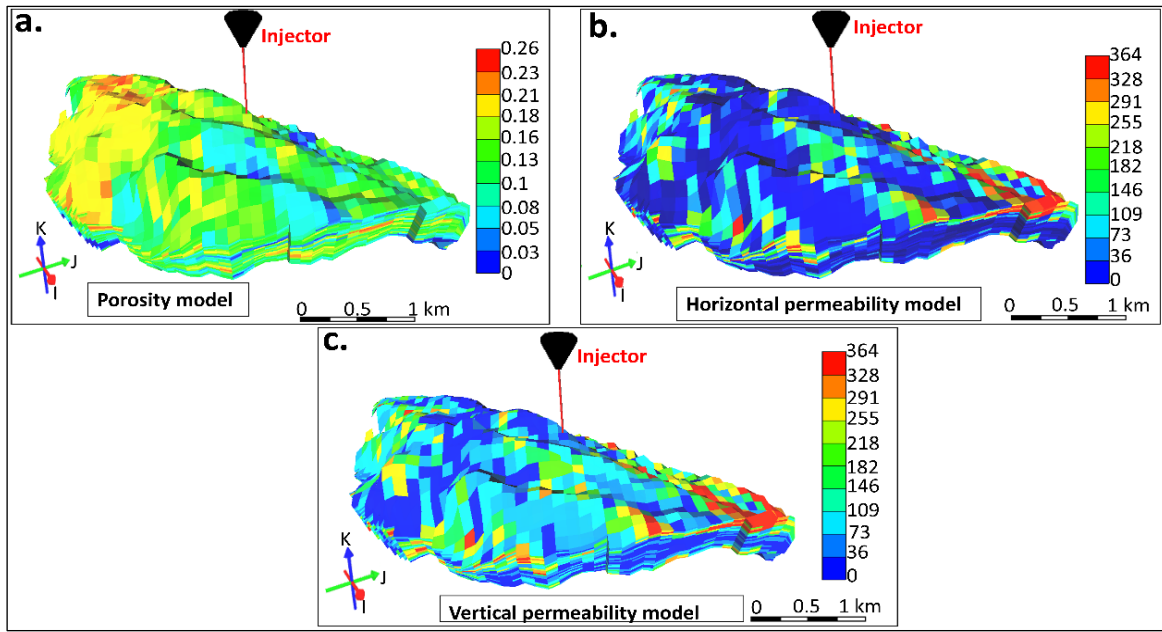


Figure 3. Land trapping model — gas saturation as a function of relative gas permeability.

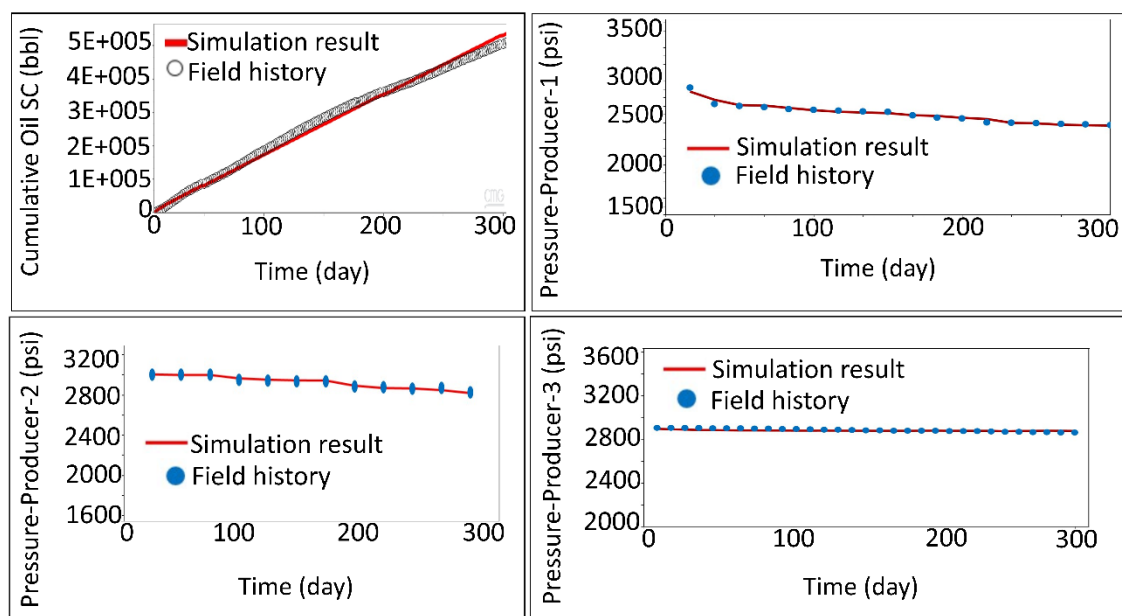
5. Simulation of CO₂-WAG sequestration

As a first step in modeling the effectiveness of WAG injection, a base case of WAG injection was modeled and compared with continuous CO₂ injection to calculate the relative effectiveness of WAG injection with respect to the specific reservoir under consideration. The base case model had 48 000 grid cells. **Figure 4** depicts the porosity and the horizontal and vertical permeability models used for the base case simulation. The anisotropy ratio of the modeled permeability was 0.7. Moreover, **Figure 5** highlights the result of cumulative oil production and pressure history matching for the reservoir model of the research area. The aquifer model represented the accurately simulated real reservoir.

In both injection scenarios (continuous CO₂ injection and WAG injection), 1.42 Mt of CO₂ was injected at a depth of 2160 m over a 20-year period. The rate of continuous CO₂ injection was set at 0.071 Mt/year at a pressure of 32 MPa. In the WAG process, the injection rate was set at 0.142 Mt/year at 32 MPa. The WAG process consisted of 10 years of CO₂ injection followed by 10 years of water injection with 60-day water injection and 60-day CO₂ injection phases. All injection scenarios were followed by a 40-year observation period during which the residual and solubility trapping capacities for CO₂ were compared.



1
2 **Figure 5.** Porosity (a), horizontal permeability (b), and vertical permeability (c) models as
3 simulated in the base case scenario.



4
5 **Figure 4. History matching result of reservoir simulation model**

6
7 Following the establishment through the above comparative analysis between continuous
8 CO₂ injection and WAG, the WAG base case was then utilized to initiate the optimization
9 procedure. Ideally, the optimization approaches were expected to enhance CO₂ trapping,
thereby maximizing CO₂ storage performance. However, accurately maximizing CO₂ trapping
using a nominal optimization workflow based on a single realization of the many plausible

1 geologic models was difficult because of varying geological uncertainties in the reservoir.
2 Hence, an integrated big-loop modeling and robust optimization workflow were proposed to
3 evaluate the expected results of the WAG process and accurately capture geological
4 uncertainties.

5 Multiple realizations of the geological model were created and ranked to accomplish this
6 robust optimization workflow. Then, the optimal solutions identified by this robust
7 optimization workflow were compared with those obtained from the nominal optimization
8 workflow to evaluate the effectiveness of the robust WAG optimization workflow. The
9 efficiency of the robust WAG optimization workflow is discussed in terms of maximizing CO₂
10 storage and reducing the risks related to the stability of the identified optimal solutions and the
11 computational costs.

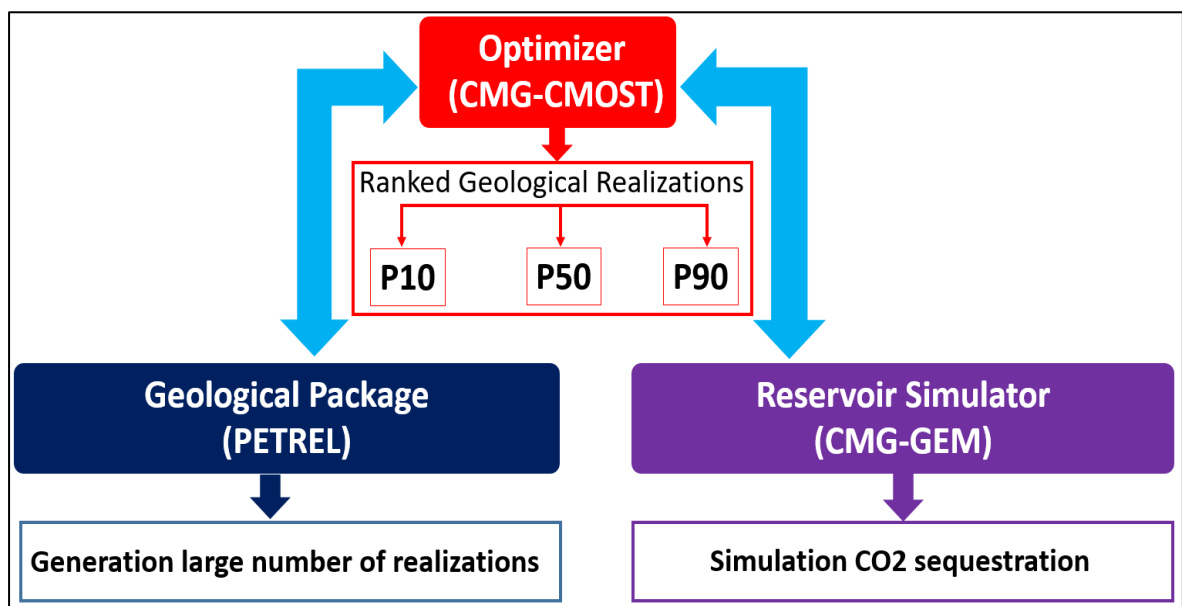
12 **5.1. Big-loop CO₂-WAG field scale modeling**

13 Generating a large number of geological realizations is necessary to capture the critical
14 effect of geology, such as porosity and permeability. The quality of complex problems,
15 such as history matching and optimization, was often enhanced by an AI optimizer to create
16 the best cooperation of different parameters based on machine learning methods. These
17 important frameworks were separated and it was difficult and waste time to include many
18 realizations geology into a reservoir model (Dang et al., 2017). Thus, a fast and automatic
19 modeling framework for the optimization of CO₂-WAG sequestration under geological
20 uncertainties is necessary. **Figure 6** highlights the big-loop modeling workflow in the
21 present study.

22 The geological model of Petrel package were automatically updated to the reservoir
23 simulator (CMG-GEM) to conduct CO₂-WAG sequestration simulation with assigned
24 group of engineering parameters. Simulation results were then investigated by the

1 intelligence optimizer (CMOST-AI) before creating the next geological models and
2 engineering parameters (water and gas cycle length). The new porosity and permeability
3 distribution were created in each step of the modeling workflow.

4 In this work, the porosity and permeability distributions are the main reservoir
5 parameters for the modeling process. The basic reservoir parameters were adapted from
6 Vo Thanh et al. (2019b) that represents a fluvial sandstone formation in Cuu Long Basin,
7 Vietnam.



8
9
10
11
12
13
Figure 6. Illustration of ranking process by integrating the geological package, reservoir
simulator and intelligence optimizer

1 **5.2.Robust optimization workflow**

2 The optimization workflow used in this study is shown in **Figure 7**. In sum, our
3 proposed robust optimization is as follows:

- 4 1. Generate geological realizations. A big-loop modeling workflow was used to
5 generate N_T geological realizations ($N_T = 200$ realizations).
- 6 2. Rank N_T geological realizations employing a reliable method. For this study, the
7 direct numerical simulations of the ranking process using a coarse grid (48 000 grid
8 cells) were completed for the 200 generated geological realizations, and the results
9 were ranked based on calculated performance (e.g., cumulative CO₂ injection). The
10 baseline WAG parameter was 60 days of water injection followed by 60 days of gas
11 injection.
- 12 3. Select a small number of representative realizations (N_R) for robust and nominal
13 optimizations. Cumulative CO₂ injection from the 200 previously generated
14 realizations was reviewed after plotting the results on the same chart. After the
15 probability of CO₂ cumulative injection distribution was reviewed, three
16 realizations (P10, P50, and P90) were ranked and selected for robust optimization.
- 17 4. Conduct optimization. The P50 CO₂ cumulative injection from point (3) was used
18 for the nominal optimization, whereas the selected N_R representative realizations
19 (P10, P50, and P90 in this study) were used to calculate the objective function for
20 robust optimization. The robust optimization is expressed as follows (Yang et al.,
21 2011):

$$J_{RO} = \frac{1}{N_r} \sum_{i=1}^{N_r} H(L, \theta_d) - r \cdot \sqrt{\frac{1}{N_R-1} \sum_{i=1}^{N_r} \left(H(L, \theta_d) - \frac{1}{N_r} \sum_{i=1}^{N_r} H(L, \theta_d) \right)^2} \quad (1)$$

1 where the robust optimization objective function is defined by J_{RO} , L is the
2 optimization parameter, θ_d is the geostatistical realization, and H is the
3 transferred function.

4 In this study, the global objective function was formulated through average CO₂
5 trapping. This objective function was adapted from other optimization study
6 (Nguyen et al., 2016). These average parameters were the sum of each geological
7 realization with the same combination divided by the number of realizations (CMG,
8 2019):

$$AverageCO_2TRAP = \frac{CO_2TRAP_1 + CO_2TRAP_2 + CO_2TRAP_3}{3} \quad (2)$$

9 where the variables CO_2TRAP_1 , CO_2TRAP_2 , and CO_2TRAP_3 are CO₂ trappings for
10 the P10, P50, and P90 geological realizations, respectively.

- 11 5. Quality control and comparative analysis. The results of the robust and nominal
12 optimization workflows were reviewed and compared for conclusive analysis and
13 field development.

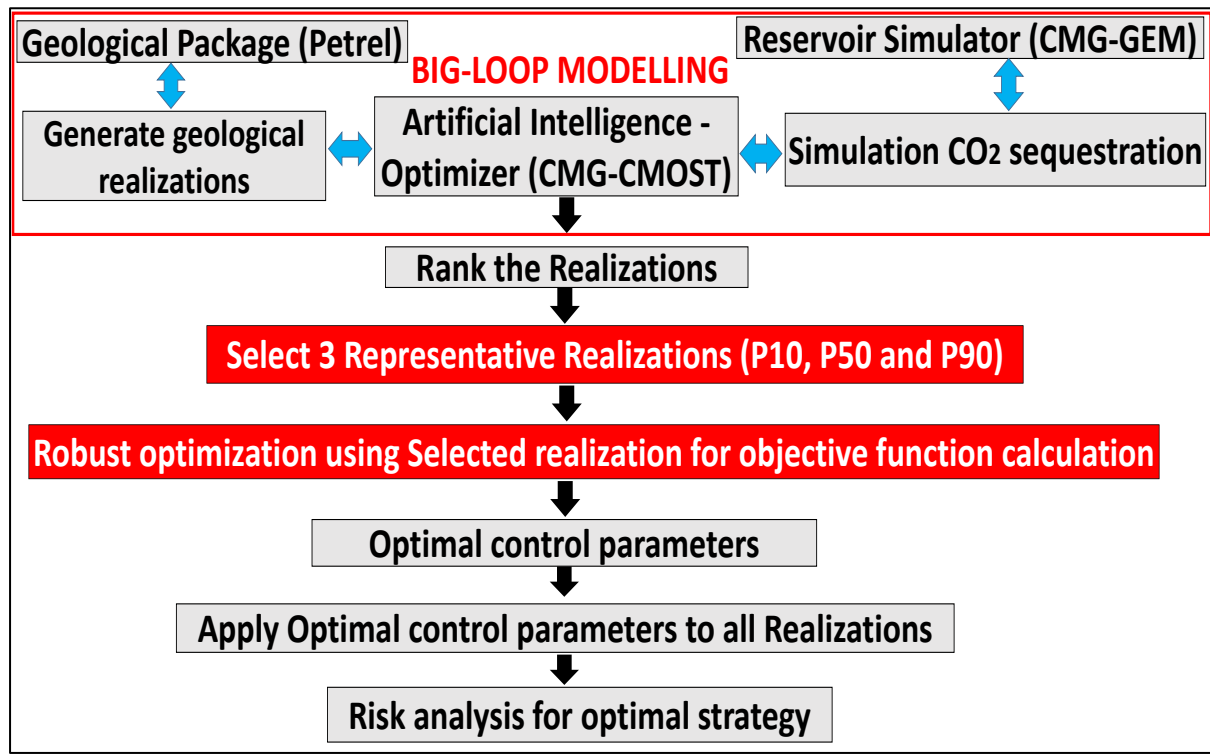


Figure 7. Optimization workflow used for this study

5.3. Optimization approaches — Design exploration and controlled evolution

(DECE) and Latin hypercube design (LHD)

For this study, the WAG process was optimized by using the experimental design method.

This method consists of (i) design exploration and controlled evolution (DECE) and (ii) Latin hypercube design (LHD). The purpose of the experimental design was to maximize the objective function using the minimum possible number of simulations.

For the DECE, simulations were created by randomly selecting levels for each parameter

through Tabu search and experimental design (Al-Mudhafar, 2016; CMG, 2019; Mckay et al., 2000; Yang et al., 2007). In the controlled evolution step, a statistical analysis of the simulation results received from the design exploration stage was conducted (CMG, 2019). A gene and allele represented each parameter and level, respectively. Analyzing which gene had notable effects on the objective function was completed by observing which allele diminished the undesirable results. This process aimed to derive the maximum amount of information from

1 the minimum number of simulation experiments. The main advantages of the DECE approach
2 were its capability to obtain an optimal solution rapidly compared with other designs of
3 experimental tools and to deviate from being trapped in local optima while inspecting
4 deactivated alleles. Moreover, DECE alleviates weak control settings that affect the objective
5 function. However, DECE cannot handle the sampling of varying probability parameters
6 during optimization (CMG, 2019). Therefore, DECE was adopted in this work for the nominal
7 optimization workflow, which was based on a single geological realization.

8 The LHD, in contrast, is a statistical sampling tool used to generate samples from input
9 parameters to develop numerous computer experiments from a multi-dimensional distribution
10 (Mckay et al., 2000). The sampling technique selects the minimum number of experiments
11 capturing several levels of variation for each parameter to provide a limited set of data points
12 that are uniformly disseminated throughout the parameter space through a space-filling design
13 (Bhat, 2001).

14 LHD is also an enhancement procedure for creating a new group of experiments in a
15 random manner if the initial dataset does not adequately represent the problem. In this study,
16 LHD was utilized to generate the simulation training dataset that was assessed by the reservoir
17 simulator to calculate the total amount of CO₂ trapping. LHD was adapted for the robust
18 optimization workflow in this study because of its statistical merits, its ability to generate
19 varying parameters (e.g., a host of uncertain geological realizations) from a scanty initial
20 dataset, and the need to lower the computational cost associated with generating bulky
21 geological realization data.

22

23

24

25

1 **6. Results**

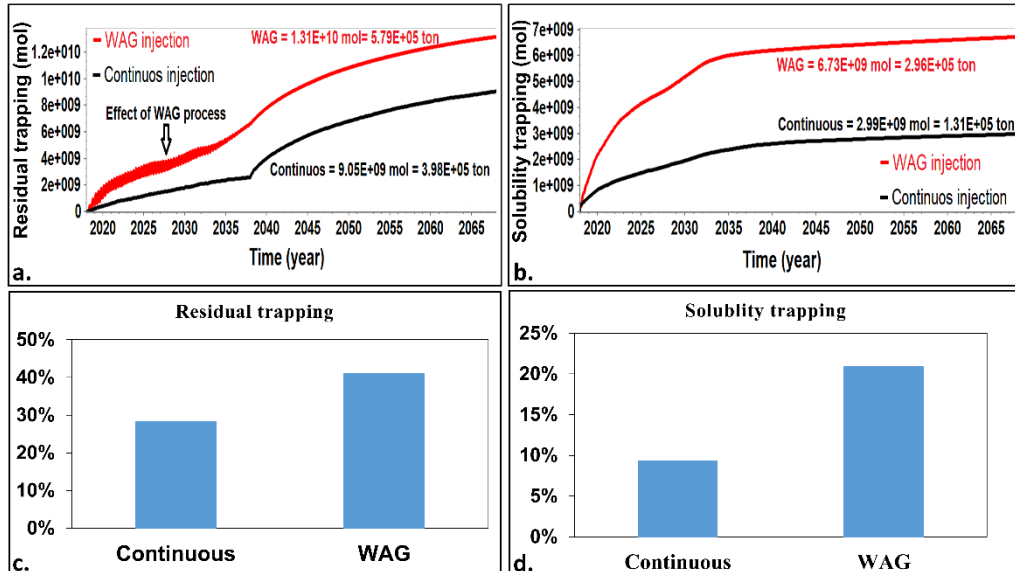
2 **6.1. Comparison between WAG and continuous CO₂ injection processes**

3 In this section, WAG was compared with continuous CO₂ injection to assess its CO₂-
4 trapping efficiency. Base-case comparisons of WAG and continuous CO₂ injections
5 demonstrated that WAG achieved a higher amount of CO₂ solubility and residual trapping than
6 continuous CO₂ injection processes. **Figure 8** highlights the extent of residual and solubility
7 CO₂ trapping for WAG injection in comparison with continuous CO₂ injection. For example,
8 the residual and dissolved CO₂ were 398 000 and 131 000 tons, respectively, in the continuous
9 injection case by the end of the simulation period. The total CO₂ trapping of continuous
10 injection was 529 000 tons. However, the WAG injection resulted in 579 000 and 296 000 tons
11 for residual and dissolved CO₂ trapping, respectively. The total CO₂ trapping of the WAG
12 process is 875 000 tons. This result demonstrated that WAG injection considerably enhances
13 CO₂-trapping efficiency.

14 Specifically, the WAG process enhanced the residual trapping by improving macro-scale
15 and micro-scale sweep efficiencies within the reservoir. WAG injection increases CO₂ trapping
16 by increasing residual CO₂ saturation and enhancing CO₂ imbibition (Herring et al., 2016). In
17 the case of improved solubility trapping during cyclical WAG injections, a larger CO₂-water
18 contact surface has increased the lateral spreading of CO₂ (Doughty, 2010).

19 CO₂ trapping in WAG and continuous injection scenarios increased rapidly after the 20-
20 year injection period and the subsequent shutting down of the well. This increase was due to
21 the migration of CO₂ after injection caused by drainage and imbibition processes. CO₂ trapping
22 led to the displacement of brine in the aquifer (drainage) at the leading end of the flow and the
23 subsequent trapping of CO₂ as brine displaced CO₂ (imbibition) (Blunt, 2018). CO₂ trapping
24 was proven to be advantageous for long-term storage, as trapped CO₂ accumulates and may

1 dissolve or react with the host rock but cannot flow and escape from the aquifer. Furthermore,
 2 Iglauer (2017) established that a significant fraction of the initial saturation of injected CO₂ can
 3 be trapped after injection, thereby limiting the migration of mobile CO₂ and reducing leakage.



4 **Figure 8.** CO₂-trapping comparison between WAG and continuous CO₂ injections:
 5 (a) & (c) residual CO₂ trapping, (b) & (d) solubility CO₂ trapping.

6.2. Optimization of CO₂ trapping

7 The length of cycles in the WAG process was considered discrete known variables,
 8 whereas porosity and permeability were treated as probable uncertain parameters to optimize
 9 the objective function (cumulative CO₂ trapping). **Table 1** presents the relevant design
 10 parameters for the WAG optimization process.

11 **Table 1.** Parameter constraints used in optimizing the WAG process.

Parameter	Lower Limit	Base case	Upper Limit	Step
Gas cycle length, days	30	60	120	10
Water cycle length, days	30	60	120	10

12
 13 Parameter constraints represented the minimum and maximum pore volume (PV) injected.
 14 We can calculate the PV injected for the range of injected CO₂ (30–120 days) by using the CO₂

1 injection rate and the reservoir PV. In this case, the PV of the reservoir is 115 518 000 m³. The
2 cumulative CO₂ injected as the base case injected within 60 days is 2 251 308 m³. The total
3 slug size is 1.95 PV when the cumulative CO₂ is divided by the PV. This procedure will act as
4 the base to calculate the lower and upper limits for the optimization process. In this case, the
5 lower limit is 0.97 PV, and the upper limit is 3.9 PV.

6 Moreover, the ranking process in this study was accomplished by integrating a geological
7 modeling software (Petrel), a compositional reservoir simulator (CMG-GEM), and an
8 optimizer (CMG-CMOST) into a single workflow (**Figure 6**). Two hundred realizations of the
9 geological model were generated from the base-case data set. A range of geological parameters,
10 including the global seed number, variogram (horizontal and vertical ranges), and azimuth
11 values, was created using the Petrel geological package (**Table 2**). Concurrently, Petrel was
12 employed to create new realizations considering the change global seed number, variogram,
13 and azimuth values while CMOST was running. These values are uncertainty parameters in
14 modeling process. Therefore, defining the minimum and maximum values to change the
15 distribution of facies, porosity, and permeability in the target reservoir was necessary.

16 **Table 2.** Parameters for the generation of geological realization.

Parameter	Lower Limit	Base case	Upper Limit	Step
HR	1000	1800	3600	200
VR	10	20	30	2
Azimuth	15	25	35	5
Global seed number	1000	8000	16000	500

17
18 Then, these realizations were automatically shifted to the reservoir simulator to perform
19 the WAG simulation and calculate the cumulative trapped CO₂ within a 20year injection

1 period. Thereafter, the reservoir simulation results were input into the optimizer, which
2 subsequently created the next geological model realization and initiated a new simulation. The
3 rate and pressure of WAG injection were kept constant for all the created realizations and were
4 the same as those for the base case.

5 **Figure 9a** depicts the cumulative CO₂ injection results for the 200 randomly generated
6 geological realizations. Moreover, **Figure 9b** shows the probability distribution function of the
7 cumulative CO₂ injection and highlights the P10, P50, and P90 realizations. Furthermore,
8 **Figures 9c–9e** show 3D images of the selected porosity and horizontal and vertical
9 permeabilities for each of the P10, P50, and P90 realizations, respectively. As shown in these
10 figures, the notable differences observed among the three sampled realizations are indicative of
11 the overall uncertainty of the studied reservoir.

12 We presented the results of the selected P10, P50, and P90 scenarios for the robust
13 optimization workflow following the methods of Al-Mudhafar et al. (2018). These authors
14 proposed a successful workflow for the robust optimization of a GAGD process by
15 investigating the three realizations to reduce risks through explicit analysis of the uncertainties
16 of the model. However, only the P50 cumulative CO₂ injection scenario was used for the
17 nominal optimization workflow. This scenario was later used for comparison with the robust
18 optimization workflow.

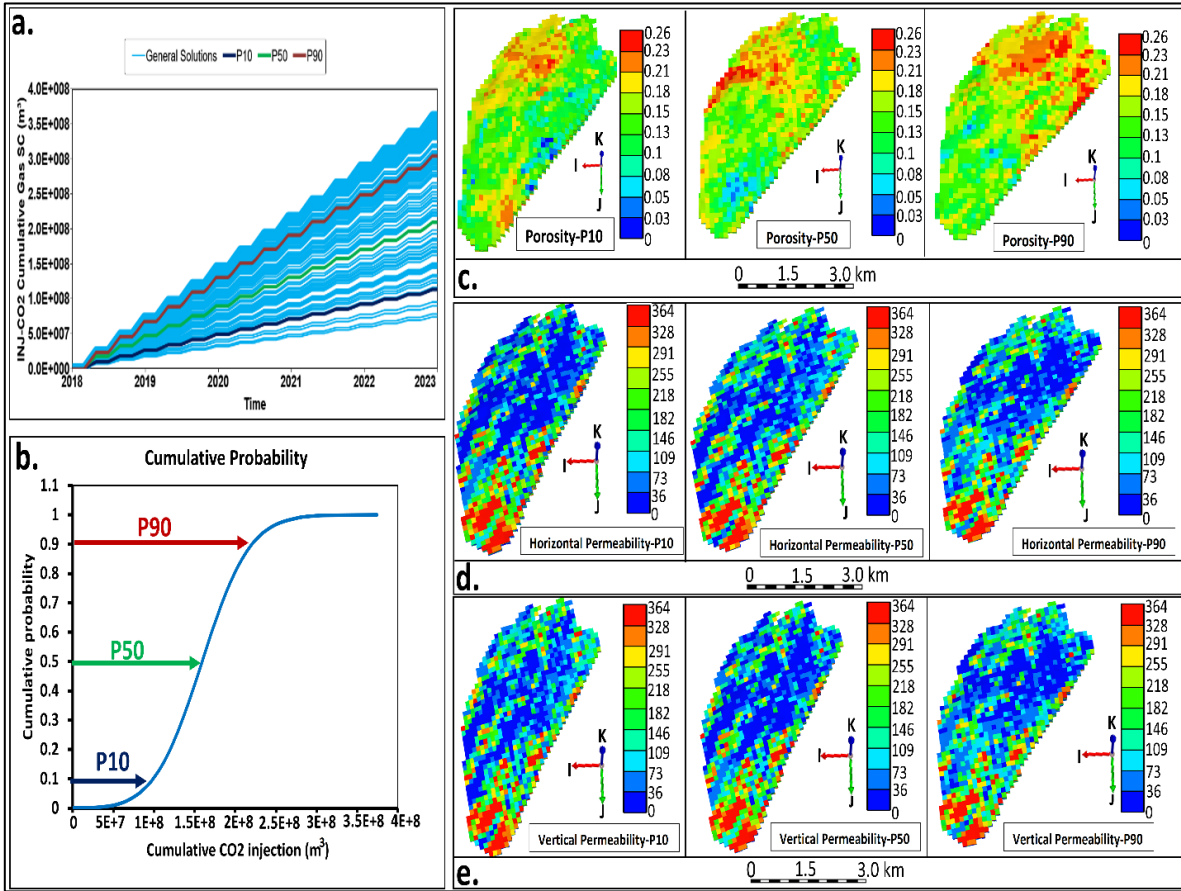


Figure 9. Results from the integrated simulation workflow: (a) plausible scenarios for the cumulative CO₂ injection, later used for the ranking process; (b) probability density function of the cumulative CO₂ injection; (c) top three ranked (P10, P50, and P90) porosity models from the generated geological realizations; (d) horizontal permeability models (P10, P50, and P90) selected from the generated geological realizations; (e) vertical permeability models (P10, P50, and P90) selected from the generated geological realizations.

6.2.1. Result of the robust optimization

The P10, P50, and P90 geostatistical realizations of porosity and permeability distributions

were used to constrain the geological models used in the robust optimization workflow. The

design parameters used to implement the robust optimization workflow are presented in

Table 1.

The robust optimization workflow investigated 250 optimal solutions from a total of 750

simulation runs across the three different realizations of the geological model. This large

1 number of simulations enabled the improvement of the robustness of the optimal solution
2 identified by the robust optimization workflow relative to the result of the nominal optimization
3 workflow. Dual-core computer (3.6 GHz, 16 GB) was used for the optimization process. The
4 CPU time of each run was 1 h and 30 min to finish one simulation job. Therefore, the main
5 issue of robust optimization workflow is computation cost. CPU resources can be upgraded to
6 reduce simulation time and solve this problem.

7 **Figures 10a** and **10c** display the amount of trapped dissolved and residual CO₂ calculated
8 for all the simulations tested as a part of the robust optimization workflow. As observed, the
9 most optimal solution (**Figure 10**, in red) exhibits the highest amount of trapped CO₂ as
10 evaluated at the end of the injection and post-injection periods. **Figures 10b** and **10d** show
11 various general solutions and the optimal solution generated by the robust optimization
12 workflow in comparison with the base case. The optimal solution, indicated by the dashed
13 purple line, defines the highest amount of trapped residual and soluble CO₂ at the end of the
14 injection and post-injection periods.

15 **Figure 11** displays the correlation between trapped CO₂ and the input WAG parameters
16 as selected for the robust optimization, demonstrating the optimal level of each variable
17 corresponding to the robust optimal solution. Herein, the optimal strategy (30/120 cycle
18 lengths) was 30 days of gas injection followed by 120 days of water injection. In the next
19 sections, results from the nominal optimization and further comparison with the robust
20 optimization are presented.

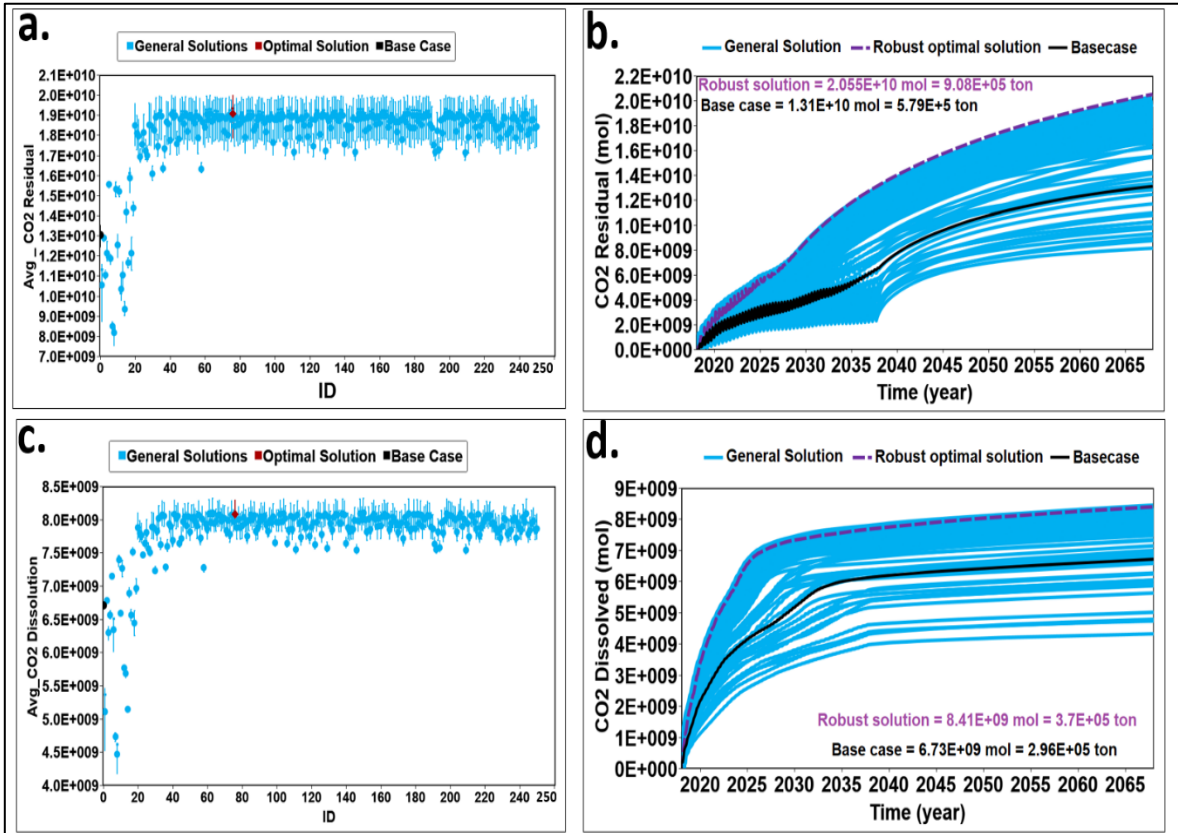


Figure 10. Trapped CO₂ as a function of the number of simulation runs showing the optimal solution (in red) — (a) trapped residual CO₂ and (b) trapped soluble CO₂; amounts of trapped (c) residual CO₂ and (d) soluble CO₂ with time.

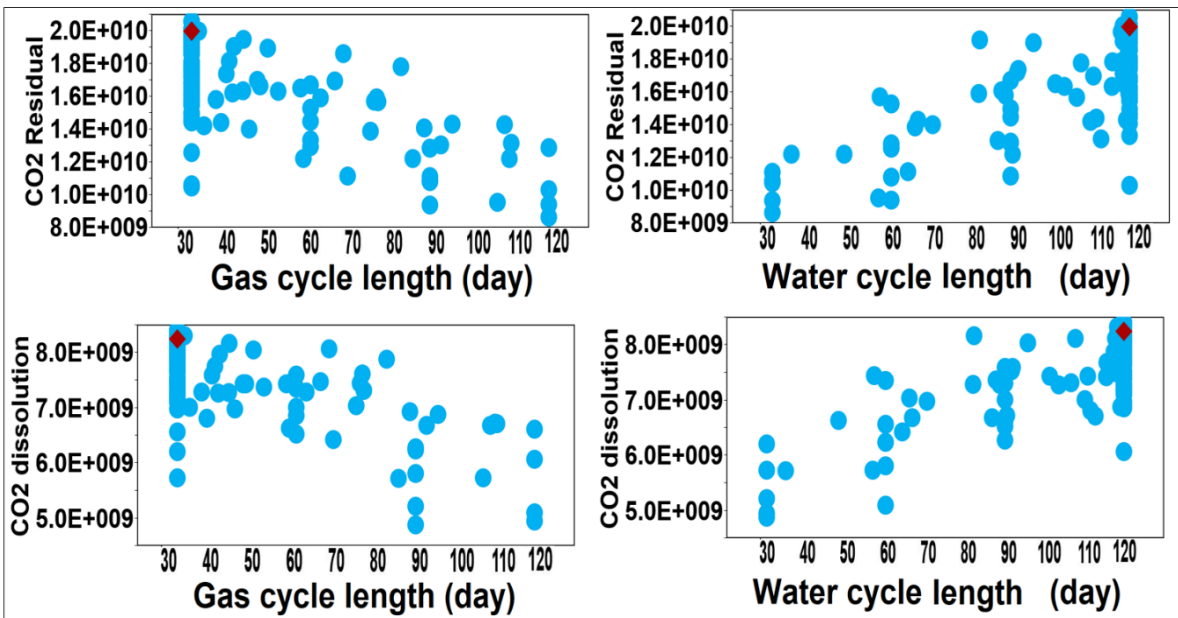
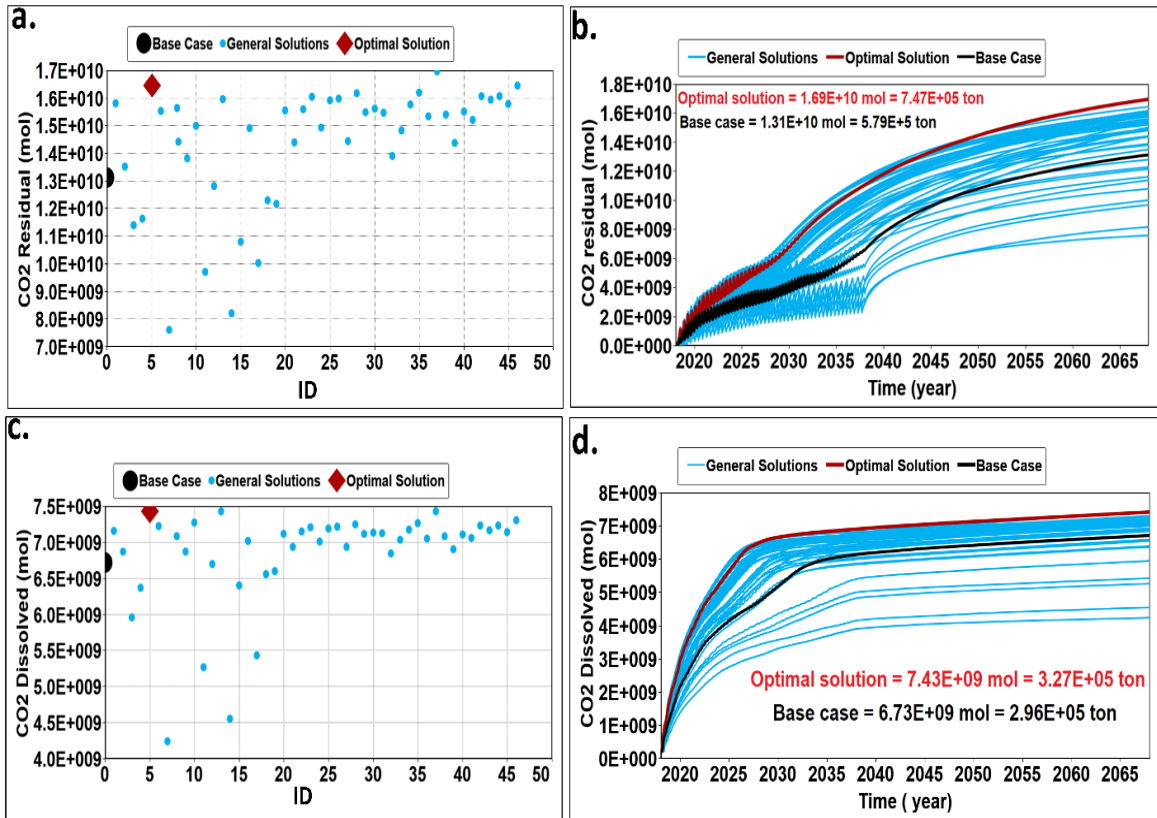


Figure 11. Cross plot depicting the relationship between the objective function (trapped CO₂) and WAG cycle length.

1 **6.2.2. Result of nominal optimization**

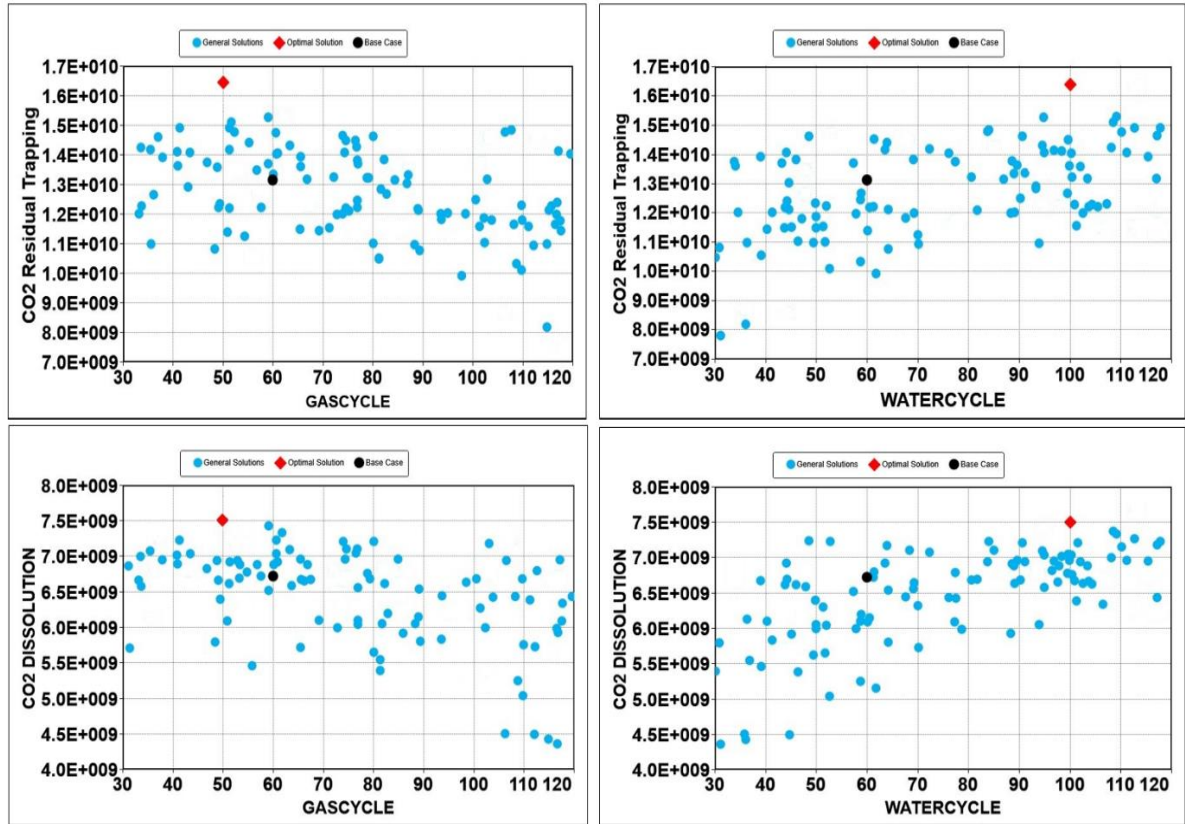
2 Similar in approach to the preceding section, this section elaborates the results from the
3 nominal optimization workflow based on the P50 geological realization to enhance the
4 performance of the WAG process relative to that calculated for the initial base case. **Figures**
5 **12a** and **12c** show the objective function based on simulation experiments from the nominal
6 optimization workflow as calculated for the 20-year injection and 40-year post-injection
7 periods. In these figures, the optimal solution was reached in a small number of simulation
8 experiments without being trapped by local optimal. Results of the base case scenario prior to
9 optimization are presented in black filled circles to validate the efficacy of the optimization
10 workflow (**Figures 12a** and **12c**). Relative to this base case scenario, the results for the
11 optimized experiments (red-filled diamonds) were improved through a series of iterative
12 experiments (blue circles, **Figures 12a** and **12c**). The amounts of trapped residual and soluble
13 CO₂ calculated for the base case and nominally optimized solution of the WAG injection are
14 shown in **Figures 12b** and **12d**, respectively.

15 The optimal solution had the highest value of residual and solubility trapping. Comparison
16 between the base case and the optimal solution based on the P50 realization of the geological
17 model demonstrated that a significant increase in CO₂ trapping can be achieved through WAG
18 process optimization. The nominal optimization values of trapped residual and soluble CO₂
19 were 747 000 and 327 000 tons, which were 168 000 and 310 000 tons more than those
20 calculated for the base case. Furthermore, **Figure 13** shows the optimal WAG parameter for
21 nominal optimization. The optimal strategy (50/100 cycle lengths) was 50 days of gas injection
22 followed by 100 days of water injection.



1
2 **Figure 12.** Right—trapped CO₂ as a function of the number of simulation runs
3 showing the nominally optimal solution (in red): (a) trapped residual CO₂ and (b)
4 trapped soluble CO₂. Left—amount of trapped (c) residual CO₂ and (d) soluble CO₂
5 with time.

1



2

3 **Figure 13.** Trapped CO₂ as a function of WAG cycle through nominal optimization:
4 gas cycle (on the left) and water cycle (on the right).

5 **6.2.3. Comparison between the robust and nominal optimization results**

6 In this section, we addressed how robust optimization is better than nominal optimization
7 by using individual analysis results for both optimizations. We sought a comparative analysis
8 between robust and nominal optimizations and explored questions to bring clarity to which
9 optimization procedure accounts for most geological uncertainties during CO₂ sequestration.
10 The ultimate goal was to determine which of these two workflows fully capture all uncertainties
11 associated with CO₂ sequestration, clarifying all operational ambiguity.

12 Therefore, two cycle lengths (30/120 and 50/100) were used to simulate three realizations
13 (P10, P50, and P90) in the case of robust optimization for effective comparison to one
14 realization (P50) in the case of nominal optimization. **Figures 14a** and **14c** depict the

1 quantitative comparison of trapped CO₂ (soluble and residual) for the nominal and robust
2 optimal solutions, respectively.

3 In all cases, the P10 of the robust optimization lies below the P50 result for nominal
4 optimization, and the P90 of the robust optimization provides the highest value for trapped
5 CO₂. A similar analysis is illustrated in **Figures 14b** and **14d** for the case of 50/100 cycle
6 lengths. Therefore, in all likelihood, the comparative results for the two optimal scenarios
7 demonstrate that the robust strategy is better than the nominal strategy because robust
8 optimization gave three different scenarios compared with the only scenario in nominal
9 optimization. Thus, robust optimization provides a flexible possibility of having more trapped
10 CO₂ (i.e., P90) by tuning geological and reservoir parameters in this direction. Furthermore,
11 five random realizations were sampled from the overall set of 200 created realizations by
12 applying our proposed workflow to effectively contrast CO₂ trapping in both optimal strategies
13 and demonstrate the robust nature of randomly generating geological realizations. **Figure 15**
14 presents the comparison of residual and dissolved CO₂ using five random realizations. As
15 observed, the 30/120 cycle lengths led to an on-average higher amount of CO₂ trapping than
16 50/100 cycle lengths in all five realizations. Moreover, 30/120 cycle lengths are recommended
17 on average over 50/100 cycle lengths during robust optimization.

18 Moreover, comparison of the results obtained from the robust optimization workflow with
19 those of the nominal optimization workflow demonstrates the greater effectiveness of the
20 robust optimization workflow in handling geological uncertainties. **Figure 16** highlights the
21 comparison of dissolved and residual-trapped CO₂ between the nominal and robust optimal
22 solutions. The robust optimization workflow with average 10th, 50th, and 90th realizations for
23 improving total CO₂ trapping (residual and dissolved) led to the output of 1.278 Mt,
24 corresponding to approximately 204 000 tons of total CO₂ trapped, which is higher than that
25 achieved by the nominal optimization workflow. For example, after a 40-year storage period,

1 90% of the CO₂ will be trapped in the optimal scenario identified by the robust optimization
2 workflow, whereas only 75% of CO₂ will be trapped in the scenario identified by the nominal
3 optimization workflow; these values correspond to the mobile CO₂ fractions of 10% and 25%,
4 respectively. Optimal WAG parameters play an important role to enhance CO₂ sequestration.
5 The cycle length of robust strategy is 30 days of gas injection followed by 120 days of water
6 injection, whereas the gas and water cycle length of nominal optimization is 50 and 100 days,
7 respectively. Hence, increasing the water cycle length can enhance CO₂ trapping and
8 dissolution in the reservoir.

9 **Figures 17a** and **17b** depict the histogram and cumulative probability distribution function
10 of the quantified uncertainty effect on CO₂ trapping to better understand the relationship
11 between geological uncertainty and CO₂ trapping. The figures also highlight the P10, P50, and
12 P90 results of the residual and solubility trapping. The wide range of calculated trapped CO₂
13 indicates the important role of quantifying the geological uncertainty in the WAG process for
14 CO₂ sequestration.

15 Moreover, **Figure 18** summarizes the CO₂ saturation for the base case and the nominal and
16 robust optimizations. As shown in these plots, the less free gas remained at the top of the
17 formation after maximizing CO₂ trapping under geological uncertainties. This result highlights
18 the manner by which robust optimization improves safety storage through either maximizing
19 the residual trapping and dissolution of CO₂ or minimizing free CO₂.

20

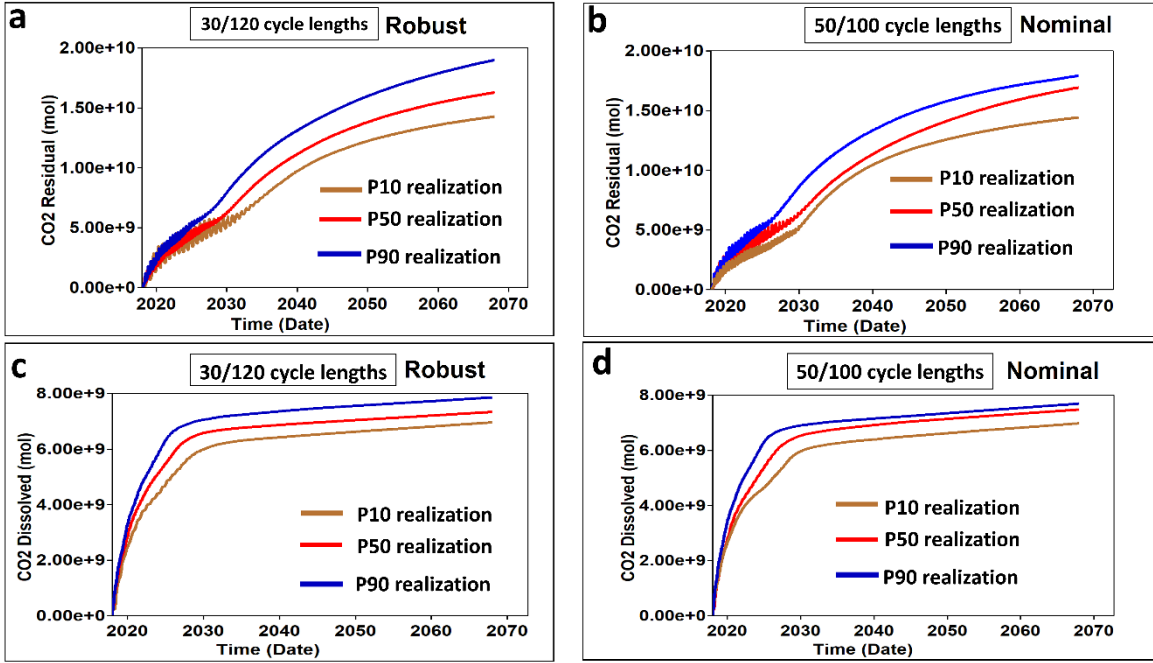


Figure 14. Nominal and robust strategies applied for three realizations (P10, P50, and P90): (a) comparative residual CO₂ trapping against time; (b) comparative soluble CO₂ trapping against time; (c) residual CO₂ trapping for the two optimal strategies; (d) solubility CO₂ trapping for the two optimal strategies.

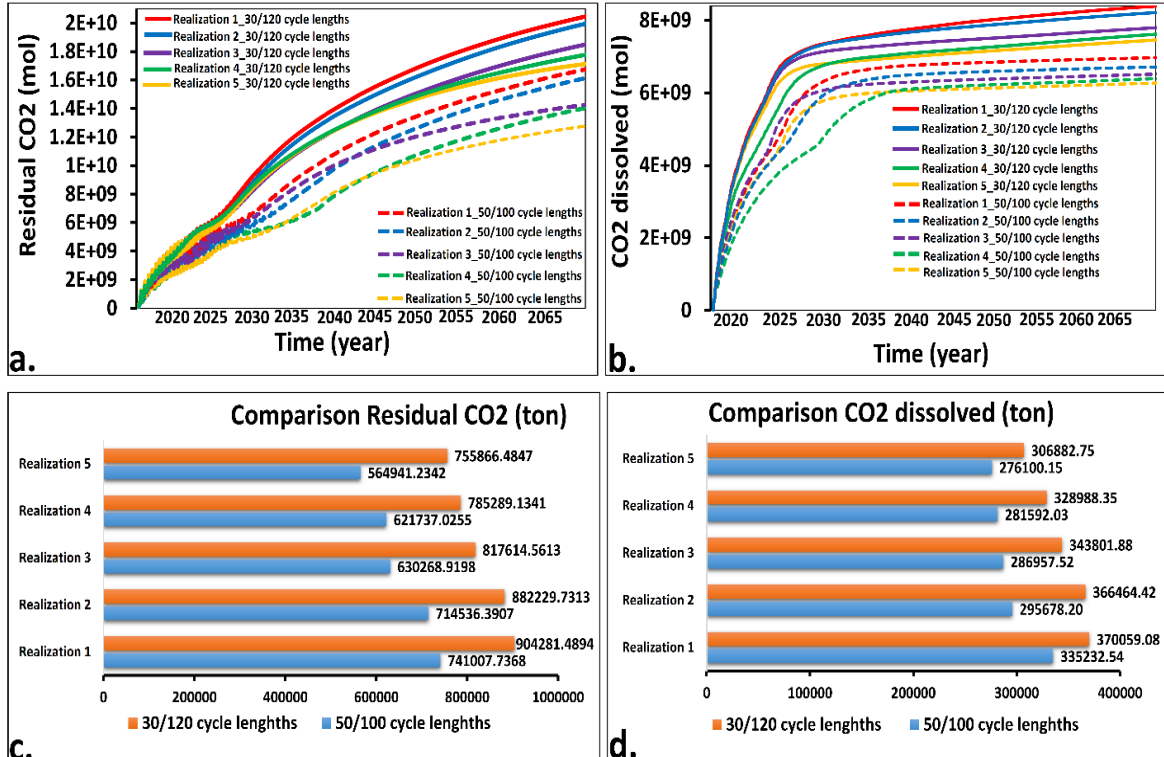


Figure 15. Robust optimization for five randomly generated geological realizations: (a) comparative residual CO₂ trapping against time; (b) comparative soluble CO₂ trapping against time; (c) amount of residual CO₂ trapped for each assessed cycle length; (d) amount of soluble CO₂ trapped for each cycle length.

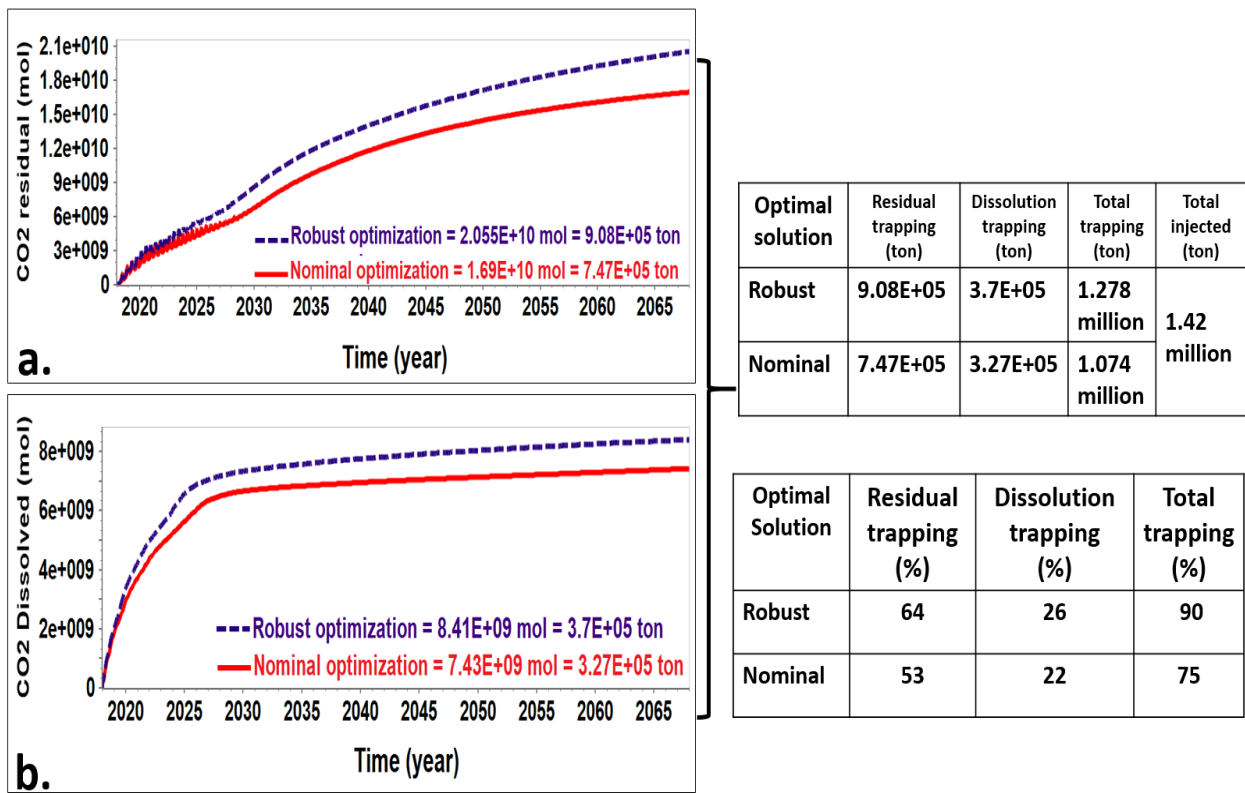


Figure 16. Comparison of CO₂ trapping results generated by the robust and nominal optimal solutions. (a) Residual trapping; (b) Dissolution trapping.

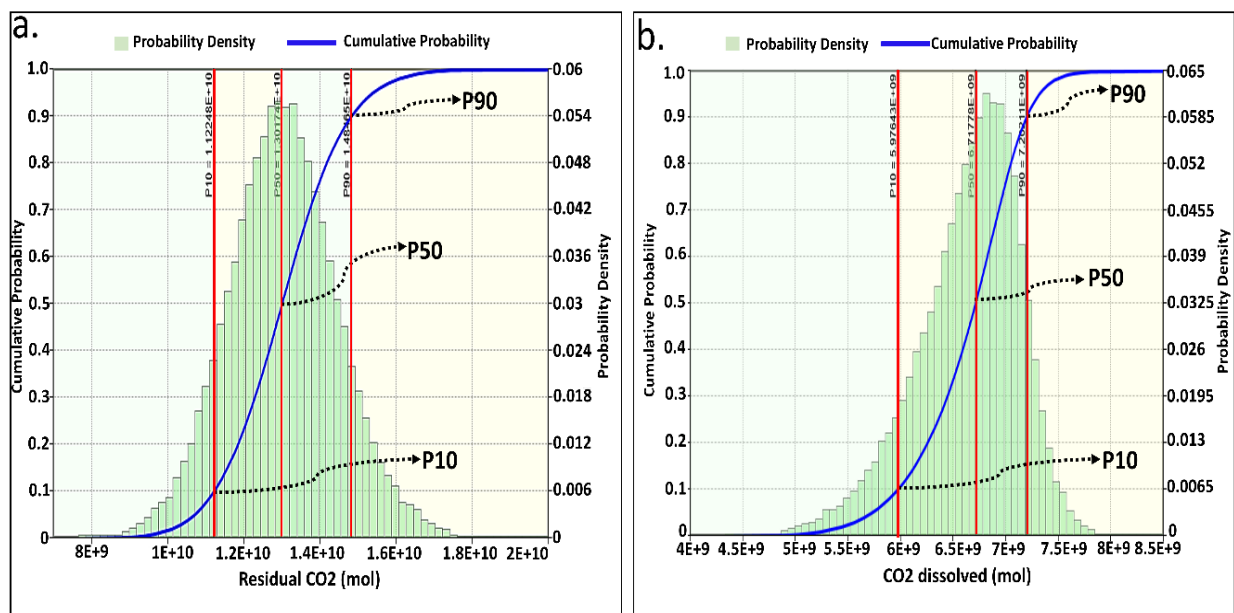


Figure 17. Uncertainty assessment for robust optimization: (a) residual CO₂ trapping; (b) dissolved CO₂ trapping.

1

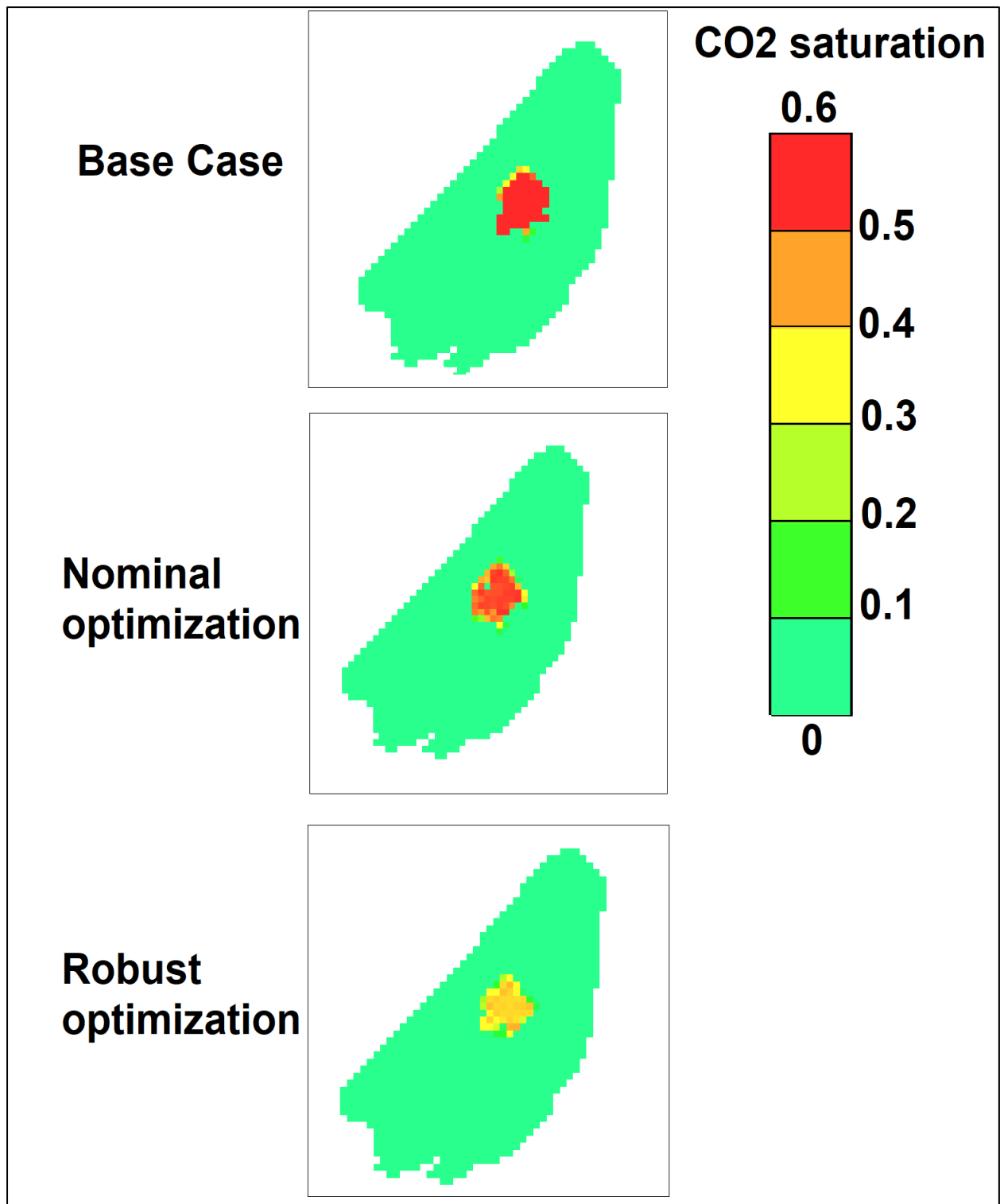


Figure 18. Free CO₂ saturation for the base case and the nominal and robust optimizations for the WAG process

2

1 **7. Discussion**

2 Our basic claim is to safeguard geological uncertainty where applicable while also ensuring
3 maximum CO₂ sequestration, and robust optimization is preferable to nominal optimization.
4 Furthermore, we propose that nominal optimization no longer fits full-scale simulation for CO₂
5 sequestration, accounting for geological uncertainty. The nominal optimization process only
6 investigates a single distribution of reservoir properties; hence, the stability of the optimization
7 result cannot be verified in light of known uncertainties in geological models. However, our
8 proposed robust optimization covers geological uncertainty, thereby eliminating any ambiguity
9 associated with CO₂ sequestration. We suggest that, at a minimum, reservoir operations (EOR
10 and CO₂ storage) should proceed in the fashion of our proposed robust optimization.

11 A notable point, despite the stated advantages of robust optimization, is concerned with
12 the daunting task of huge geological models associated with high computational times and
13 costs. Hence, the following considerations must be taken into account: (1) capturing the effects
14 of geological uncertainty parameters and (2) optimizing computation costs and runtime based
15 on available computational resources. Additionally, the number of ranked geological
16 realizations, specific to particular fields, necessary to complete a robust optimization workflow
17 depends on factors such as the geologic structure of the reservoir, the number of grid cells in
18 the reservoir model, and the computational capacity of the available computer resources.

19 In conclusion, our work proposed the integrated modeling and robust optimization
20 workflow to enhance CO₂ storage efficiency under geological uncertainties in a heterogeneous
21 fluvial sandstone reservoir. The presented workflow can be employed to improve CO₂-trapping
22 capacity within other real-scale field projects. This methodology can also be used in different
23 aspects of CO₂ storage, EOR, and other engineering.

24

25

1 **8. Conclusions**

2 This paper presented a robust optimization workflow to determine the optimal strategy
3 of the WAG process for CO₂ sequestration in a heterogeneous fluvial sandstone
4 reservoir. The following key observations can be drawn from our results:

- 5 • The base case of WAG injection improved total CO₂ trapping by approximately
6 25% compared with the continuous CO₂ injection process.
- 7 • Nominal optimization used 50 days of gas injection and 100 days of water
8 injection, whereas the robust optimization used 30 days of gas injection and 120
9 days of water injection. We demonstrated that the strategy recommended by the
10 robust optimization (i.e., 30/120 cycle lengths) is better than the strategy
11 supported by the nominal optimization (i.e., 50/100 cycle lengths) based on a
12 variety of metrics. Thus, the robust optimization method (using three
13 realizations) is superior to the nominal optimization method (using only one
14 realization). Therefore, the proposed robust optimization framework can
15 improve CO₂-trapping efficiency and reduce project risks in light of geological
16 uncertainties.
- 17 • Nominal optimization led to 13% enhanced total CO₂ trapping over the WAG
18 base case. However, the robust optimal solution increased the total CO₂ trapping
19 by 15% over the nominal optimization case (28% larger than the WAG base
20 case). More specifically, the base case and the nominal and robust optimizations
21 of the WAG process led to a total trapping of 0.875, 1.074, and 1.278 Mt of
22 CO₂, respectively. All these results reflect the necessity of considering
23 geological uncertainties in the optimization framework of the WAG injection
24 application in real reservoir evaluations.

1

2 **Acknowledgments**

3 The authors would like to express their gratitude to the Japanese International Cooperation
4 Agency for their financial support and to the Computer Modeling Group for their support in
5 the use of CMG-GEM and CMOST.

6

7

8

9

10

11

12

13

14

15

16

17

18

19

20

21

1

2

Abbreviations

AI	Artificial Intelligence
ASP	Akaline–Surfactant–Polymer
CCS	Carbon Capture and Storage
CO ₂	Carbon Dioxide
CMG	Computer Modeling Group
CMOST	Intelligent Optimization and Analysis Tool
CPU	Central Processing Unit
DECE	Design Exploration and Controlled Evolution
EOR	Enhance Oil Recovery
IOR	Improve Oil Recovery
GAGD	Gas-Assisted Gravity Drainage
GB	Gigabyte
GCS	Geological Carbon Storage
GEM	Compositional and Unconventional Simulator
GHz	Gigahertz
LHD	Latin Hypercube Design
MPa	Megapascal
Mt	Million tons
N _R	Representative geological realizations
N _T	Geological realizations
Petrel	Exploration and Production Software Platform
HR	Horizontal Range
SAGD	Steam-Assisted Gravity Drainage
sc	Supercritical
T	Time
VR	Vertical Range

3

4

5

1 **References**

- 2 Al-khdheeawi, E.A., Vialle, S., Barifcani, A., Sarmadivaleh, M., Iglauer, S., 2018. Effect of
3 wettability heterogeneity and reservoir temperature on CO₂ storage efficiency in deep
4 saline aquifers. *Int. J. Greenh. Gas Control* 68, 216–229.
5 <https://doi.org/10.1016/j.ijggc.2017.11.016>
- 6 Al-Khdheeawi, E.A., Vialle, S., Barifcani, A., Sarmadivaleh, M., Iglauer, S., 2018a. Enhance-
7 ment of CO₂ trapping efficiency in heterogeneous reservoirs by water-alternating
8 gas injection. *Greenh. Gases Sci. Technol.* 12, 1–12. <https://doi.org/10.1002/ghg.1805>
- 9 Al-Khdheeawi, E.A., Vialle, S., Barifcani, A., Sarmadivaleh, M., Iglauer, S., 2017. Effect of
10 brine salinity on CO₂ plume migration and trapping capacity in deep saline aquifers.
11 *APPEA J.* 57, 100–109.
- 12 Al-Khdheeawi, E.A., Vialle, S., Barifcani, A., Sarmadivaleh, M., Zhang, Y., Iglauer, S., 2018b. Impact of salinity on CO₂ containment security in highly heterogeneous reservoirs.
13 *Greenh. Gases Sci. Technol.* 8, 93–105. <https://doi.org/10.1002/ghg.1723>
- 14 Al-Menhal, A., Niu, B., Krevor, S., 2015. Capillarity and wetting of carbon dioxide and brine
15 during drainage in Berea sandstone at reservoir conditions. *Water Resour. Res.* 51, 7895–
16 7914. <https://doi.org/10.1002/2014WR015608>.Received
- 17 Al-Mudhafar, W., 2016. Statistical Reservoir Characterization, Simulation, And Optimization
18 Of Field Scale-Gas Assisted Gravity Drainage (Gagd) Process With Uncertainty
19 Assessments. PhD thesis. Louisiana State University and Agricultural and Mechanical
20 College
- 21 Al-Mudhafar, W.J., Rao, D.N., Srinivasan, S., 2018. Robust Optimization of Cyclic CO₂
22 flooding through the Gas-Assisted Gravity Drainage process under geological
23 uncertainties. *J. Pet. Sci. Eng.* 166, 490–509. <https://doi.org/10.1016/j.petrol.2018.03.044>
- 24 Aminu, M.D., Nabavi, S.A., Rochelle, C.A., Manovic, V., 2017. A review of developments in
25 carbon dioxide storage. *Appl. Energy* 208, 1389–1419.
26 <https://doi.org/10.1016/j.apenergy.2017.09.015>
- 27 Ampomah, W., Balch, R., Will, R., Cather, M., Gunda, D., Dai, Z., 2017. Co-optimization of
28 CO₂-EOR and Storage Processes under Geological Uncertainty. *Energy Procedia* 114,
29 6928–6941. <https://doi.org/10.1016/j.egypro.2017.03.1835>
- 30 Ampomah, W., Balch, R.S., Cather, M., Will, R., Gunda, D., Dai, Z., Soltanian, M.R., 2017. Optimum design of CO₂storage and oil recovery under geological uncertainty. *Appl.*
31 *Energy* 195, 80–92. <https://doi.org/10.1016/j.apenergy.2017.03.017>
- 32 B.J.O.L. McPherson, Cole, B.S., 2000. Multiphase CO₂ flow, transport and sequestration in
33 the Powder River Basin, Wyoming, USA. *J. Geochem. Explor.* 69–70, 65.
- 34 Bachu, S., 2002. Sequestration of CO₂ in geological media in response to climate change: Road
35 map for site selection using the transform of the geological space into the CO₂ phase
36 space. *Energy Convers. Manag.* 43, 87–102. [https://doi.org/10.1016/S0196-8904\(01\)00009-7](https://doi.org/10.1016/S0196-8904(01)00009-7)
- 37 Bachu, S., 2000. Sequestration of CO₂ in geological media: Criteria and approach for site
38 selection in response to climate change. *Energy Convers. Manag.* 41, 953–970.
- 39

- 1 [https://doi.org/10.1016/S0196-8904\(99\)00149-1](https://doi.org/10.1016/S0196-8904(99)00149-1)
- 2 Bachu, S., Gunter, W.D., Perkins, E.H., 1994. Aquifer disposal of CO₂: Hydrodynamic and
3 mineral trapping. *Energy Convers. Manag.* 35, 269–279. [https://doi.org/10.1016/0196-8904\(94\)90060-4](https://doi.org/10.1016/0196-8904(94)90060-4)
- 5 Bhat, C.R., 2001. Quasi-random maximum simulated likelihood estimation of the mixed
6 multinomial logit model. *Transp. Res. Part B* 35, 677–693.
- 7 Blunt, M.J., 2018. Multiphase Flow in Permeable Media. A Pore-Scale Perspective,
8 Groundwater. Cambridge University Press. <https://doi.org/10.1111/gwat.12812>
- 9 Brooks, R.H., Corey, A.T., 1964. Hydraulic Properties Of Porous Media. *Hydrol. Pap.* 3, Color.
10 State Univ. Fort Collins 27. <https://doi.org/citeulike-article-id:711012>
- 11 Bruant, R.G., Jr., J., Celia, M.A., Guswa, A.J., Peters, C.A., 2002. Peer Reviewed: Safe Storage
12 of CO₂ in Deep Saline Aquifiers. *Environ. Sci. Technol.* 36, 240A–245A.
13 <https://doi.org/10.1021/es0223325>
- 14 Christensen, J.R., Stenby, E.H., Skauge, A., 2001. Review of WAG Field Experience. *SPE*
15 *Reserv. Eval. Eng.* 4, 97–106. <https://doi.org/10.2118/71203-PA>
- 16 CMG, 2019. Manual of Computer Modelling Group's Software. Calgary, Cananda.
- 17 Dai, Z., Viswanathan, H., Middleton, R., Pan, F., Ampomah, W., Yang, C., Jia, W., Xiao, T.,
18 Lee, S., Mcpherson, B., Balch, R., Grigg, R., White, M., 2016. CO₂ Accounting and Risk
19 Analysis for CO₂ Sequestration at Enhanced Oil Recovery Sites.
20 <https://doi.org/10.1021/acs.est.6b01744>
- 21 Dai, Z., Zhang, Y., Bielicki, J., Amooie, M.A., Zhang, M., Yang, C., Zou, Y., Ampomah, W.,
22 Xiao, T., Jia, W., Middleton, R., Zhang, W., Sun, Y., Moortgat, J., Soltanian, M.R.,
23 Stauffer, P., 2018. Heterogeneity-assisted carbon dioxide storage in marine sediments.
24 *Appl. Energy* 225, 876–883. <https://doi.org/10.1016/j.apenergy.2018.05.038>
- 25 Dang, C., Nghiem, L., Nguyen, N., Chen, Z., Nguyen, Q., 2016. Evaluation of CO₂Low
26 Salinity Water-Alternating-Gas for enhanced oil recovery. *J. Nat. Gas Sci. Eng.* 35, 237–
27 258. <https://doi.org/10.1016/j.jngse.2016.08.018>
- 28 Dang, C., Nghiem, L., Nguyen, N., Chen, Z., Yang, C., Nguyen, Q., 2017. A framework for
29 assisted history matching and robust optimization of low salinity water flooding under
30 geological uncertainties. *J. Pet. Sci. Eng.* 152, 330–352.
31 <https://doi.org/10.1016/j.petrol.2017.03.009>
- 32 Dang, C., Nghiem, L., Nguyen, N., Yang, C., Chen, Z., Bae, W., 2018. Modeling and
33 optimization of alkaline-surfactant-polymer flooding and hybrid enhanced oil recovery
34 processes. *J. Pet. Sci. Eng.* 169, 578–601. <https://doi.org/10.1016/j.petrol.2018.06.017>
- 35 Doughty, C., 2010. Investigation of CO₂ plume behavior for a large-scale pilot test of geologic
36 carbon storage in a saline formation. *Transp. Porous Media* 82, 49–76.
37 <https://doi.org/10.1007/s11242-009-9396-z>
- 38 Doughty, C., 2007. Modeling geologic storage of carbon dioxide: Comparison of non-
39 hysteretic and hysteretic characteristic curves. *Energy Convers. Manag.* 48, 1768–1781.
40 <https://doi.org/10.1016/j.enconman.2007.01.022>
- 41 Ennis-King, J., Paterson, L., 2005. Role of convective mixing in the long-term storage of
42 carbon dioxide in deep saline formations. *SPE J.* 10, 349–356.

- 1 <https://doi.org/10.2118/84344-PA>
- 2 Eshraghi, S.E., Rasaei, M.R., Zendehboudi, S., 2016. Optimization of miscible CO₂ EOR and
3 storage using heuristic methods combined with capacitance/resistance and Gentil
4 fractional flow models. *J. Nat. Gas Sci. Eng.* 32, 304–318.
5 <https://doi.org/10.1016/j.jngse.2016.04.012>
- 6 Ettehadtavakkol, A., Lake, L.W., Bryant, S.L., 2014. CO₂-EOR and storage design
7 optimization. *Int. J. Greenh. Gas Control* 25, 79–92.
8 <https://doi.org/10.1016/j.ijggc.2014.04.006>
- 9 Fedutenko, E., Yang, C., Card, C., Nghiem, L., 2013. Optimization of SAGD Process
10 Accounting for Geological Uncertainties Using proxy Models, in: CPSG/CESG/CWLS
11 Geoconvention. Calgary, AB, Canada.
- 12 Flett, M., Gurton, R., Weir, G., 2007. Heterogeneous saline formations for carbon dioxide
13 disposal: Impact of varying heterogeneity on containment and trapping. *J. Pet. Sci. Eng.*
14 57, 106–118. <https://doi.org/10.1016/j.petrol.2006.08.016>
- 15 Foroud, T., Seifi, A., AminShahidy, B., 2016. An efficient optimization process for
16 hydrocarbon production in presence of geological uncertainty using a clustering method:
17 A case study on Brugge field. *J. Nat. Gas Sci. Eng.* 32, 476–490.
18 <https://doi.org/10.1016/j.jngse.2016.04.059>
- 19 Gaus, I., 2010. Role and impact of CO₂-rock interactions during CO₂ storage in sedimentary
20 rocks. *Int. J. Greenh. Gas Control* 4, 73–89. <https://doi.org/10.1016/j.ijggc.2009.09.015>
- 21 Genuchten, V.A.N., 1980. A Closed-form Equation for Predicting the Hydraulic Conductivity
22 of Unsaturated Soils 1. *Soil Sci. Soc. Am. J.* 44, 892–898.
- 23 Hassanzadeh, H., Pooladi-Darvish, M., Keith, D.W., 2009. Accelerating CO₂ dissolution in
24 saline aquifers for geological storage - Mechanistic and sensitivity studies. *Energy and
25 Fuels* 23, 3328–3336. <https://doi.org/10.1021/ef900125m>
- 26 Herring, A.L., Andersson, L., Wildenschild, D., 2016. Enhancing residual trapping of
27 supercritical CO₂ via cyclic injections. *Geophys. Res. Lett.* 43, 9677–9685.
28 <https://doi.org/10.1002/2016GL070304>. Received
- 29 Hesse, M.A., Woods, A.W., 2010. Buoyant dispersal of CO₂ during geological storage.
30 *Geophys. Res. Lett.* 37, 1–5. <https://doi.org/10.1029/2009GL041128>
- 31 Holloway, S., Savage, D., 1993. The potential for aquifer disposal of carbon dioxide in the UK.
32 *Geotherm. Energy* 34, 925–932.
- 33 Hung, N. Du, Le, H. Van, 2004. Petroleum Geology of Cuu Long Basin - Offshore Vietnam,
34 in: Proceedings of AAPG International Conference. Barcelona, Spain, September 21-24.
- 35 Iglauer, S., 2017. CO₂-Water-Rock Wettability: Variability, Influencing Factors, and
36 Implications for CO₂Geostorage. *Acc. Chem. Res.* 50, 1134–1142.
37 <https://doi.org/10.1021/acs.accounts.6b00602>
- 38 Iglauer, S., Al-yaseri, A.Z., Rezaee, R., Lebedev, M., 2015. Storage Capacity and Containment
39 Security. *Geophys. Res. Lett.* 42, 9279–9284. <https://doi.org/10.1002/2015GL065787>
- 40 Iglauer, S., Paluszny, A., Pentland, C.H., Blunt, M.J., 2011. Residual CO₂ imaged with X-ray
41 micro-tomography. *Geophys. Res. Lett.* 38, 1–6. <https://doi.org/10.1029/2011GL049680>
- 42 IPCC, 2005. IPCC special report on carbon dioxide capture and storage. Cambridge University

- 1 Press.
- 2 Jesmani, M., Jafarpour, B., Bellout, M.C., Foss, B., 2020. A reduced random sampling strategy
3 for fast robust well placement optimization. *J. Pet. Sci. Eng.* 184, 106414.
4 <https://doi.org/10.1016/j.petrol.2019.106414>
- 5 Juanes, R., Spiteri, E.J., Orr, F.M., Blunt, M.J., 2006. Impact of relative permeability hysteresis
6 on geological CO₂storage. *Water Resour. Res.* 42, 1–13.
7 <https://doi.org/10.1029/2005WR004806>
- 8 Kumar, A., Ozah, R., Noh, M., Pope, G.A., Bryant, S., Sepehrnoori, K., Lake, L.W., 2005.
9 Reservoir Simulation of CO₂ Storage in Deep Saline Aquifers. *SPE J.* 10, 336–348.
10 <https://doi.org/10.2118/89343-PA>
- 11 Lackner, K.S., 2003. A guide to CO₂ sequestration. *Science* (80-.). 300, 1677–1678.
12 <https://doi.org/10.1126/science.1079033>
- 13 Land, C.S., 1968. Calculation of Imbibition Relative Permeability for Two- and Three-Phase
14 Flow From Rock Properties. *Soc. Pet. Eng. J.* 8, 149–156. <https://doi.org/10.2118/1942-pa>
- 16 Li, Y., Li, J., Ding, S., Zhang, H., 2016. Co-optimization of CO₂sequestration and enhanced
17 oil recovery in extra-low permeability reservoir in Shanbei. *Energy Sources, Part A*
18 Recover. Util. Environ. Eff.
- 19 Mac Dowell, N., Fennell, P.S., Shah, N., Maitland, G.C., 2017. The role of CO₂ capture and
20 utilization in mitigating climate change. *Nat. Clim. Chang.* 7, 243–249.
21 <https://doi.org/10.1038/nclimate3231>
- 22 Mckay, M.D., Beckman, R.J., Conover, W.J., 2000. A comparison of three methods for
23 selecting values of input variables in the analysis of output from a computer code.
24 *Technometrics* (JSTOR Abstr. 42, 55–61).
- 25 Meng, Q., Jiang, X., 2014. Numerical analyses of the solubility trapping of CO₂ storage in
26 geological formations. *Appl. Energy* 130, 581–591.
27 <https://doi.org/10.1016/j.apenergy.2014.01.037>
- 28 Min, B., Sun, A.Y., Wheeler, M.F., Jeong, H., 2018. Utilization of multiobjective optimization
29 for pulse testing dataset from a CO₂-EOR/sequestration field. *J. Pet. Sci. Eng.* 170, 244–
30 266. <https://doi.org/10.1016/j.petrol.2018.06.035>
- 31 Morley, C.K., 2002. A tectonic model for the Tertiary evolution of strike-slip faults and rift
32 basins in SE Asia. *Tectonophysics* 347, 189–215. [https://doi.org/10.1016/S0040-1951\(02\)00061-6](https://doi.org/10.1016/S0040-1951(02)00061-6)
- 34 Naylor, M., Wilkinson, M., Haszeldine, R.S., 2011. Calculation of CO₂ column heights in
35 depleted gas fields from known pre-production gas column heights. *Mar. Pet. Geol.* 28,
36 1083–1093. <https://doi.org/10.1016/j.marpgeo.2010.10.005>
- 37 Nguyen, N.T.B., Dang, C.T.Q., Nghiem, L.X., Chen, Z., Li, H., 2016. Robust Optimization of
38 Unconventional Reservoirs under Uncertainties. *SPE Eur. Featur.* 78th EAGE Conf.
39 Exhib. <https://doi.org/10.2118/180108-MS>
- 40 Nwachukwu, A., Jeong, H., Sun, A., Pyrcz, M., Lake, L.W., 2018. Machine Learning-Based
41 Optimization of Well Locations and WAG Parameters under Geologic Uncertainty, in:
42 *SPE Improved Oil Recovery Conference*. Tulsa, Oklahoma, USA, 14-18 April 2018.

- 1 <https://doi.org/10.2118/190239-ms>
- 2 Petvipsit, K.R., Elsheikh, A.H., Laforce, T.C., King, P.R., Blunt, M.J., 2014. Robust
3 optimisation of CO₂ sequestration strategies under geological uncertainty using adaptive
4 sparse grid surrogates. *Comput. Geosci.* 18, 763–778. <https://doi.org/10.1007/s10596-014-9425-z>
- 5 Pinto, J.W.O., Afonso, S.M.B., Willmersdorf, R.B., 2019. Robust optimization formulations
6 for waterflooding management under geological uncertainties. *J. Brazilian Soc. Mech.
7 Sci. Eng.* 41. <https://doi.org/10.1007/s40430-019-1970-x>
- 8 Rasmusson, K., Rasmusson, M., Tsang, Y., Niemi, A., 2016. A simulation study of the effect
9 of trapping model, geological heterogeneity and injection strategies on CO₂ trapping. *Int.
10 J. Greenh. Gas Control* 52, 52–72. <https://doi.org/10.1016/j.ijggc.2016.06.020>
- 11 Safarzadeh, M.A., Motahhari, S.M., 2014. Co-optimization of carbon dioxide storage and
12 enhanced oil recovery in oil reservoirs using a multi-objective genetic algorithm (NSGA-II). *Pet. Sci.* 11, 460–468. <https://doi.org/10.1007/s12182-014-0362-1>
- 13 Schmidt, W.J., Hoang, B.H., Handschy, J.W., Hai, V.T., Cuong, T.X., Tung, N.T., 2019.
14 Tectonic evolution and regional setting of the Cuu Long Basin, Vietnam. *Tectonophysics*
15 757, 36–57. <https://doi.org/10.1016/j.tecto.2019.03.001>
- 16 Shamshiri, H., Jafarpour, B., 2012. Controlled CO₂ injection into heterogeneous geologic
17 formations for improved solubility and residual trapping. *Water Resour. Res.* 48, 1–15.
18 <https://doi.org/10.1029/2011WR010455>
- 19 Sibawaihi, N., Awotunde, A.A., Sultan, A.S., Al-Yousef, H.Y., 2015. Sensitivity studies and
20 stochastic optimization of CO₂ foam flooding. *Comput. Geosci.* 19, 31–47.
<https://doi.org/10.1007/s10596-014-9446-7>
- 21 Song, Z., Li, Z., Wei, M., Lai, F., Bai, B., 2014. Sensitivity analysis of water-alternating-
22 CO₂ flooding for enhanced oil recovery in high water cut oil reservoirs. *Comput. Fluids*
23 99, 93–103. <https://doi.org/10.1016/j.compfluid.2014.03.022>
- 24 Span, R., Wagner, W., 1996. A new equation of state for carbon dioxide covering the fluid
25 region from the triple-point temperature to 1100 K at pressures up to 800 MPa. *J. Phys.
26 Chem. Ref. Data* 25, 1509–1596. <https://doi.org/10.1063/1.555991>
- 27 Spiteri, E., Juanes, R., Blunt, M.J., Orr, F.M., 2005. Relative-Permeability Hysteresis:
28 Trapping Models and Application to Geological CO₂ Sequestration. *SPE Annu. Tech.
29 Conf. Exhib.* <https://doi.org/10.2118/96448-MS>
- 30 Spycher, N., Pruess, K., 2005. CO₂-H₂O mixtures in the geological sequestration of CO₂. II.
31 Partitioning in chloride brines at 12–100°C and up to 600 bar. *Geochim. Cosmochim. Acta*
32 69, 3309–3320. <https://doi.org/10.1016/j.gca.2005.01.015>
- 33 Van Essen, G., Zandvliet, M., Van den Hof, P., Bosgra, O., Jansen, J.-D., 2009. Robust
34 Waterflooding Optimization of Multiple Geological Scenarios. *SPE J.* 14, 24–27.
35 <https://doi.org/10.2118/102913-PA>
- 36 Vo Thanh, H., Sugai, Y., Nguele, R., Sasaki, K., 2019a. Integrated work flow in 3D geological
37 model construction for evaluation of CO₂ storage capacity of a fractured basement
38 reservoir in Cuu Long Basin, Vietnam. *Int. J. Greenh. Gas Control* 90, 102826.
39 <https://doi.org/10.1016/j.ijggc.2019.102826>

- 1 Vo Thanh, H., Sugai, Y., Sasaki, K., 2019b. Impact of a new geological modelling method on
2 the enhancement of the CO₂ storage assessment of E sequence of Nam Vang field,
3 offshore Vietnam. Energy Sources, Part A Recover. Util. Environ. Eff. 41, 1–14.
4 <https://doi.org/10.1080/15567036.2019.1604865>
- 5 Welkenhuysen, K., Rupert, J., Compernolle, T., Ramirez, A., Swennen, R., Piessens, K., 2017.
6 Considering economic and geological uncertainty in the simulation of realistic investment
7 decisions for CO₂-EOR projects in the North Sea. Appl. Energy 185, 745–761.
8 <https://doi.org/10.1016/j.apenergy.2016.10.105>
- 9 Xu, T., Apps, J.A., Pruess, K., 2004. Numerical simulation of CO₂disposal by mineral trapping
10 in deep aquifers. Appl. Geochemistry 19, 917–936.
11 <https://doi.org/10.1016/j.apgeochem.2003.11.003>
- 12 Yan, W., Huang, S., Stenby, E.H., 2011. Measurement and modeling of CO₂ solubility in
13 NaCl brine and CO₂ -saturated NaCl brine density. Int. J. Greenh. Gas Control 5, 1460–
14 1477. <https://doi.org/10.1016/j.ijggc.2011.08.004>
- 15 Yang, C., Card, C., Nghiem, L., Fedutenko, E., 2011. Robust Optimization of SAGD
16 Operations under Geological Uncertainties. Proc. SPE Reserv. Simul. Symp. 21–23.
17 <https://doi.org/10.2118/141676-MS>
- 18 Yang, C., Nghiem, L., Card, C., Bremeier, M., 2007. Reservoir Model Uncertainty
19 Quantification T hrough Computer-Assisted History Matching.
- 20 Yasari, E., Pishvaie, M.R., 2015. Pareto-based robust optimization of water-flooding using
21 multiple realizations. J. Pet. Sci. Eng. 132, 18–27.
22 <https://doi.org/10.1016/j.petrol.2015.04.038>
- 23 Zhang, Z., Agarwal, R., 2013. Numerical simulation and optimization of CO₂ sequestration in
24 saline aquifers. Comput. Fluids 80, 79–87.
25 <https://doi.org/10.1016/j.compfluid.2012.04.027>
- 26 Zhong, Z., Liu, S., Carr, T.R., Takbiri-Borujeni, A., Kazemi, M., Fu, Q., 2019. Numerical
27 simulation of Water-alternating-gas Process for Optimizing EOR and Carbon Storage.
28 Energy Procedia 158, 6079–6086. <https://doi.org/10.1016/j.egypro.2019.01.507>
- 29